

SEISMIC STUDIES ON THE GRID WESTERN HALF OF THE ROSS ICE SHELF:
RIGGS I AND RIGGS II

James D. Robertson

ARCO Oil and Gas Company, Dallas, Texas 75221

Charles R. Bentley

Geophysical and Polar Research Center, University of Wisconsin,
Madison, Wisconsin 53706

Abstract. Airlifted geophysical surveys were carried out on the grid western half of the Ross Ice Shelf, Antarctica, during the austral summers of 1973-1974 and 1974-1975, as part of the Ross Ice Shelf Geophysical and Glaciological Survey (RIGGS). Seismic reflection records were obtained at 76 stations, seismic short-refraction records at nine stations, seismic long-refraction records at four stations, radar-sounding reflection records at 93 stations, and gravity measurements at 89 stations. The seismic results, supplemented by radar-sounding measurements of ice thickness, are discussed here. The P wave velocity increases from about 500 m s^{-1} at the surface to $3811 \pm 7 \text{ m s}^{-1}$ at depths of 70-80 m in the ice, and the S wave velocity increases from about 300 m s^{-1} at the surface to about 1970 m s^{-1} at 60 m. The maximum P wave velocity is significantly lower than the maximum velocity (3850 m s^{-1}) in grounded ice sheets at the same mean annual surface temperature. The average P wave velocity through the ice shelf is $3688 \pm 15 \text{ m s}^{-1}$. Densities and elastic moduli computed from seismic velocities are consistent with densities measured on ice cores and elastic moduli determined in laboratory experiments on ice. Significant depths in the densification process of the firn have been located by analysis of the seismic velocity gradients at $11 \pm 2 \text{ m}$ (the "critical depth"), $25 \pm 10 \text{ m}$ (significance uncertain), and $46 \pm 8 \text{ m}$ (the firn-ice boundary). There is S wave velocity anisotropy in the firn that probably is caused by layered structure, but comparison between seismic and radar echo times shows no evidence of an average preferred orientation of crystallographic c axes in the body of the ice shelf. A complete listing of ice and water layer thicknesses and ocean bottom elevations is given. These results have already been discussed elsewhere. Sea bottom

slopes are locally similar to regional slopes, which suggests that the seabed is relatively smooth at wavelengths of a few kilometers. Interval velocities and acoustic impedances in the layer of sediment at the seafloor match those expected for unconsolidated glacial marine till. A seismic reflector at a depth of 50-150 m within the till probably correlates with a glacial erosional surface previously discovered in sediments in the Ross Sea. The best estimate of the P wave velocity in seismic basement at long-refraction seismic stations is $5.5-5.7 \text{ km s}^{-1}$. One or two kilometers of lower-velocity rocks and sediments overlie basement beneath three floating stations; on Crary Ice Rise basement lies about three quarters of a kilometer beneath the ice.

Contents

Introduction.....	56
Physical Properties of the Ross Ice Shelf	
Near-surface compressional and shear	
wave velocities.....	56
Maximum compressional and shear wave	
velocities.....	58
Average compressional wave velocity ..	63
Density and elastic moduli	64
Densification horizons derived from	
seismic velocity gradients	66
Anisotropy	68
Ice Thickness and Sea-Bottom Topography..	71
Survey results	71
Sea bottom slopes	74
Sub-Bottom Characteristics	74
Interval velocity	74
Sea-bottom reflection coefficients and	
acoustic impedances	76
Long refraction studies	76
Summary	81

TABLE 1. Summary of Seismic and Surface Radar Measurements, RIGGS I and II

	RIGGS I (1973-1974)	RIGGS II (1974-1975)	Total
Seismic reflection stations	39	37	76
P wave short-refraction profiles	7	3	10
S wave short-refraction profiles	6	2	8
Long-refraction profiles	2	2	4
Seismic wide-angle ice bottom reflection stations	4	5	9
Sediment interval velocity determinations	3	1	4
Sea bottom slope determinations	3	6	9
Sea bottom reflection coefficient determinations	4	5	9
Surface radar-sounding stations	55	38	93

Introduction

The experiments discussed in this paper were carried out during the Ross Ice Shelf Geophysical and Glaciological Survey (RIGGS) field seasons from December 15, 1973, to February 3, 1974 (RIGGS I), and from November 22, 1974, to January 27, 1975 (RIGGS II). For a summary of RIGGS see Bentley, [1984]. Herein we analyze the seismic data (Table 1) in full; radar results are introduced as needed to aid interpretation. The major topics covered are (1) the physical properties of the ice shelf, (2) ice thickness and subglacial ocean depth, and (3) the character of the ocean floor.

In general, airlifted stations were occupied during good weather, and geophysical work was conducted around the base camps during poor weather. Remote survey stations were occupied by two teams of three or four geophysicists each, the teams occupying alternate stations. The basic series of measurements taken at a remote site consisted of seismic reflection shots, radar soundings, and gravity readings. Whenever possible, radar and gravity profiling were conducted locally around the site. At selected stations, more extensive experiments, such as wide-angle radar and seismic soundings and short refraction shooting, were performed.

Seismic shots were recorded on two Texas Instruments model 7000B 24-trace seismic systems during RIGGS I and on one model 7000B and one SIE model RS-49R 24-trace seismic system during RIGGS II. Two Randall Electronics (SPRI Mark II) 35-MHz radar-sounding systems were used to make radar measurements, supplemented during RIGGS II by a 150-MHz radar system built by the University of Wisconsin Department of Electrical Engineering.

In addition to the main text, this paper includes several appendices, containing extensive site-by-site data and other supplementary information, on microfiche (back pocket of this book).

Physical Properties of the Ross Ice Shelf

Near-Surface Compressional and Shear Wave Velocities

Velocities of both compressional (P) and shear (S) waves, designated v_p and v_s , respectively, increase rapidly as functions of depth in the upper 50 m of the ice shelf owing to the compaction and recrystallization of annual snow layers into ice. Below the firn-ice boundary at about 50 m the increase is steady but slower until, at 80 m or so, the velocities attain their maximum values. Velocities decrease downward through the lower shelf, despite a slow increase in density, owing to the increase of temperature with depth [Gow, 1963; Clough and Hansen, 1979]. The bottom surface of the floating shelf is necessarily at the freezing point of seawater, whereas the mean annual surface temperatures in the survey area of RIGGS I and II average about -26°C [Thomas, 1976; Crary et al., 1962a; b]. The best estimates of the temperature coefficients of v_p and v_s in ice are $-2.3 \text{ m s}^{-1} \text{ K}^{-1}$ and $-1.2 \text{ m s}^{-1} \text{ K}^{-1}$, respectively [Kohnen, 1974], indicating a probable decrease in v_p of more than 50 m s^{-1} and in v_s of more than 25 m s^{-1} in the lower part of the Ross Ice Shelf.

An important consequence of the existence of an internal seismic velocity maximum is that the complete velocity-depth function in the ice shelf cannot be determined directly. Short-refraction profiles can be used to determine only the velocity structure down to the velocity maximum: below that, only the average velocity between the velocity maximum and the bottom of the ice can be determined (from oblique reflection soundings).

Ten P wave short-refraction profiles were recorded at the following nine sites during RIGGS I and II: H7, H11S, I10S, J7S, J9DS, K11, P5, the RIGGS I base camp (BC), and the RIGGS II base camp (RI). Station locations are shown in Figure 1. Station J9DS, about half a kilometer grid southwest of station

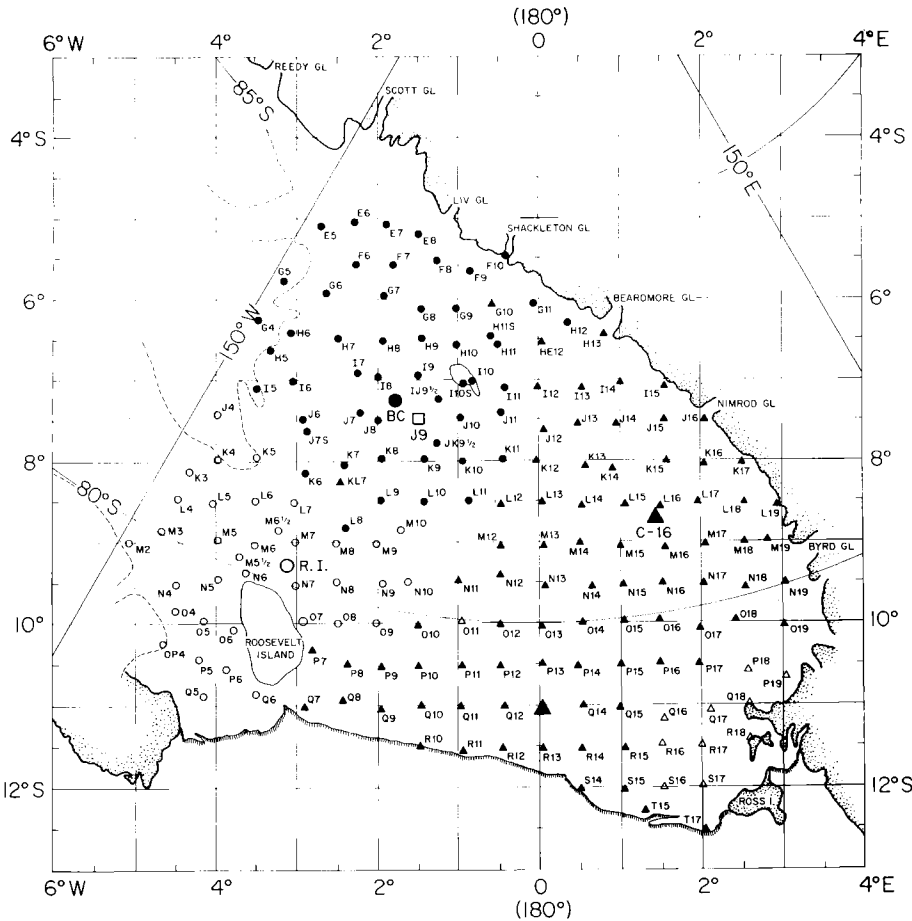


Fig. 1. Map of RIGGS stations [from Bentley, 1984]. Stations occupied during RIGGS I and II are indicated by solid circles and open circles, respectively. Stations J9DS and J9DC are at essentially the same location as station J9. In the rectangular grid coordinate system shown, meridians are parallel to the Greenwich meridian, with grid north toward Greenwich. The origin of the system is at the South Pole, and 1° of grid latitude or longitude equals 1° of geographic latitude.

J9, designates the site selected for the Ross Ice Shelf Project (RISP) drilling through the ice shelf. Two profiles were recorded at BC, one (BC-A) parallel to a glaciological strain line between BC and J9 and the other (BC-B) perpendicular to BC-A. S wave short-refraction profiles, including two at BC, were recorded at all P wave short-refraction sites except J7S and J9DS.

The normal field procedure was to lay out a 24-geophone, 2-m-interval in-line spread and to shoot blasting caps (for P) or hit a 4" x 4" stake transversely (for S) at both ends of the spread and at distances to 50, 100, 150, 200, and 250 m from one end. Two shots usually were fired (or hit) at each distance, and shots were recorded at the fastest available paper speed, about 0.8 m s^{-1} for the 7000B systems and 0.6 m s^{-1} for the RS-49R system, to provide maximum

resolution of first breaks. Shot instants were provided by a geophone placed next to the stake or on a metal plate over the cap.

Travel times were picked to a precision of 0.1 ms with the aid of a seven-power measuring magnifier; the accuracy of the travel times is estimated to be 0.3 ms. Graphs of travel time versus distance were plotted and observed to possess the smoothly varying curved shape, concave toward the distance axis, that is characteristic of refraction profiling in the dry snow zone of an ice sheet. At nearly all stations, P wave travel time data were extended beyond the limit of the short-refraction records by picking first P arrivals from long-refraction or reflection seismograms. Instrumental calibration corrections have been applied as discussed in Appendix A (on microfiche).

Short-refraction travel times were con-

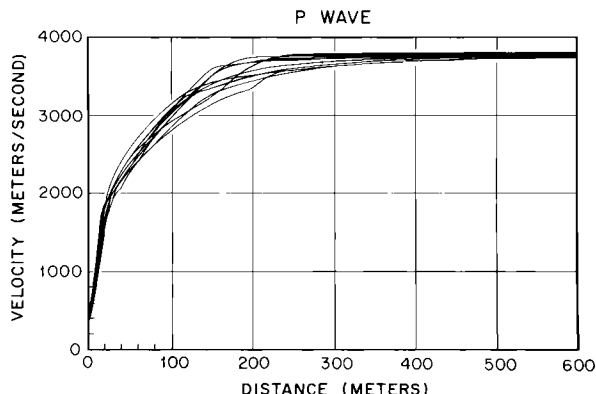


Fig. 2. Apparent v_p versus distance at 10 short-refraction stations. (Two curves are indistinguishable in this plot.)

verted to velocities versus depth through the intermediate step of computing apparent seismic velocity (the velocity with which a wave appears to travel along a line of geophones), as a function of distance. The apparent velocity at any point is equal to the inverse of the slope of the travel time curve at that point. Slopes may be obtained graphically or numerically. Particular numerical differentiation techniques that we tested were (1) the three-point central difference approximation, (2) fitting of least squares straight lines to sets of data points, and (3) least squares fitting of a second-degree polynomial to a set of data points followed by analytical differentiation of the polynomial.

After some experimentation, we chose the graphical method for determining slopes at distances of less than 200-300 m, where the curvature of the travel time is noticeable, and numerical method 2 for larger distances. (Method 1 was too unstable for accurate results, whereas method 3 did not yield a sufficiently good fit to the observed data.) Slopes were plotted against distance and smoothed graphically.

Curves of apparent velocity versus distance for the short-refraction sites are shown in Figures 2 and 3. Discrete values of velocity versus distance at each site are listed in Appendix B1 (on microfiche).

Since seismic velocities increase with density [Robin, 1958] and densities, averaged over a seismic wavelength (about a meter), increase uniformly with depth in the ice shelf [Gow, 1963], we can safely assume that the seismic velocities are continuous, monotonically increasing functions of depth. Thus the velocity-distance data could be converted to velocity-depth data by means of the Wiechert-Herglotz-Bateman (WHB) integral (see, e.g., Grant and West, [1965, p. 138]):

$$z_i = \frac{1}{\pi} \int_0^{x_i} \cosh^{-1} (pv_i) dx \quad (1)$$

where v_i is v_p or v_s at depth z_i as observed at distance x_i and p is the slope of the travel time curve at distance $x < x_i$.

A computer program called WHB was written to evaluate equation (1) by fitting a second-degree Lagrange polynomial to sets of three values of the inverse hyperbolic cosine. The mathematics of the numerical integration and a listing, explanation, and test of the program were presented by Robertson [1975]. The velocity-depth output is presented graphically in Figures 4 (v_p) and 5 (v_s) and tabulated in Appendix B1 (microfiche). The estimated standard error in individual values of velocity for both v_p and v_s is $\pm 30 \text{ m s}^{-1}$ at the surface diminishing to $\pm 20 \text{ m s}^{-1}$ at 20 m and to $\pm 10 \text{ m s}^{-1}$ at 50 m.

There is an increase in v_p from about 500 m s^{-1} at the surface to about 3800 m s^{-1} at depths of 70 or 80 m; v_s ranges from about 300 m s^{-1} at the surface to about 1970 m s^{-1} at 60 m. (Because of the very gradual velocity gradients near the velocity maxima, it is not certain that the indicated difference in depth to maximum v_p and to maximum v_s is real.) Values averaged over all the profiles on the grid western part of the Ross Ice Shelf are listed in Table 2.

Maximum Compressional and Shear Wave Velocities

As was previously mentioned, density and temperature changes in the ice shelf combine to produce a maximum in seismic velocities. We designate the maximum velocity in general by v_{\max} , or specifically for P and S waves, by $(v_p)_{\max}$ and $(v_s)_{\max}$, respectively. There are several ways to calculate v_{\max} : (1) one

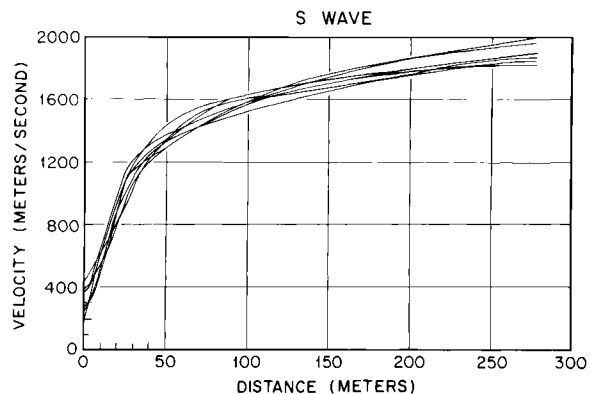


Fig. 3. Apparent v_s versus distance at eight short-refraction stations. (Two curves are indistinguishable in this plot.)

TABLE 2. Average Wave Velocities and Densities Calculated From v_p as a Function of Depth

Depth, m	v_p , m s^{-1}	v_s , m s^{-1}	ρ , kg m^{-3}
0	440 ± 30	304 ± 32	344 ± 3
2.5	999 ± 33	547 ± 20	392 ± 3
5	1472 ± 41	755 ± 16	442 ± 5
10	2112 ± 25	1116 ± 16	529 ± 4
15	2456 ± 27	1343 ± 14	587 ± 5
20	2709 ± 29	1489 ± 13	637 ± 6
25	2928 ± 29	1592 ± 11	684 ± 7
30	3119 ± 31	1666 ± 11	730 ± 8
35	3284 ± 31	1729 ± 11	772 ± 8
40	3420 ± 30	1782 ± 11	808 ± 8
45	3533 ± 31	1828 ± 12	838 ± 9
50	3618 ± 28	1869 ± 14	861 ± 8
55	3679 ± 24		877 ± 6
60	3719 ± 20		887 ± 5
65	3744 ± 15		894 ± 4
70	3763 ± 11		898 ± 3

The error estimates for the velocities are standard errors in the means; for the densities they correspond to the standard error in v_p propagated through equation (2).

may construct a travel time plot using several shots at distances greater than that at which v_{\max} is expected first to be observed; the slope of the plot, which should be a straight line, is $(v_{\max})^{-1}$; (2) a cross-spread velocity may be calculated for a single shot at a sufficient distance from the spread; (3) multiple surface reflections from shots at great distances may be picked; the interval between successive surface multiples is equal to the time intercept of the maximum velocity line extrapolated linearly back to zero distance.

To implement method 1, a minimum distance for sampling v_{\max} must be chosen. We will call that distance x_{\min} . Crary et al. [1962a; b] proposed 100 m as the depth of maximum seismic velocity in the Ross Ice Shelf. To sample this depth, the shot-geophone distance on the surface should be at least 5 or 6 times the depth, or 500 or 600 m. A more conservative choice of x_{\min} is 1000 m. Several seismic shots at distances greater than 600 m were recorded at stations BC, H12, I10S, and RI. Values of $(v_p)_{\max}$ at those stations calculated by the least squares technique assuming $x_{\min} = 600$ m and $x_{\max} = 1000$ m are presented in Table 3. There is no significant difference between the two sets of results. There do, however, appear to be significant differences between stations: in particular, $(v_p)_{\max}$ at station RI is significantly higher than that at station BC (by $44 \pm 8 \text{ m s}^{-1}$), even though

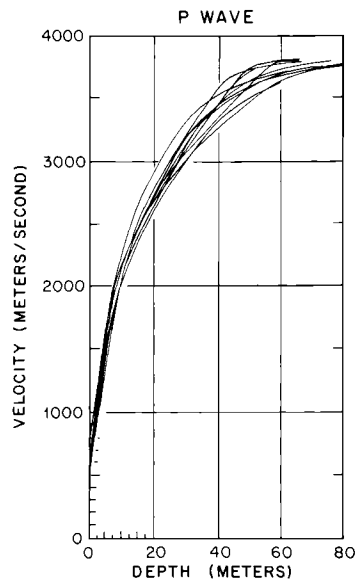


Fig. 4. P wave velocity versus depth at short-refraction stations.

both profiles were reversed. Since it is $(v_p)_{\max}$ at station RI that is out of line with the others and with previous measurements [Crary et al., 1962a], we suggest that there may be some effect of crystalline anisotropy there. The average value of $(v_p)_{\max}$ at the other three stations is $3796 \pm 4 \text{ m s}^{-1}$ for $x_{\min} = 600$ m; if we include station RI, the mean is $3811 \pm 11 \text{ m s}^{-1}$.

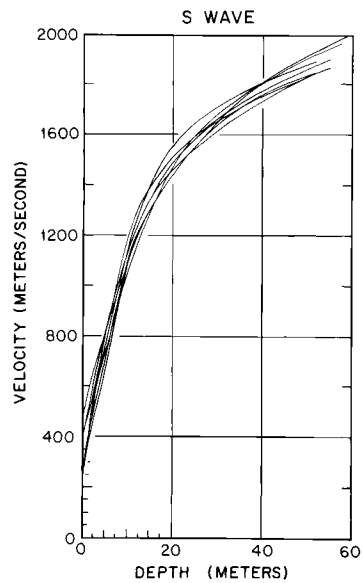


Fig. 5. S wave velocity versus depth at short-refraction stations. (Two curves are indistinguishable in this plot.)

TABLE 3. Values of $(v_p)_{\max}$ From Travel Time Plots

Station	Shot Locations	Maximum Distance, m	Minimum Distance, m	Intercept, ms	$(v_p)_{\max}$, m s ⁻¹	Minimum Distance, m	Intercept, ms	$(v_p)_{\max}$, m s ⁻¹
BC	W	2340	624	58	23	3771 ± 5	1000	3803 ± 3
	E	1342	629	41	31	3816 ± 8	49	3896 ± 8
Mean (BC)						3794 ± 7		3796 ± 20
H12 I10S		2770	600	134	24	3800 ± 4	1008	3803 ± 3
		4396	613	66	26	3789 ± 6	1005	3789 ± 8
RI	W	4869	611	74	33	3869 ± 3	1022	3836 ± 2
	E	4865	621	47	27	3807 ± 4		
Mean (RI)						3838 ± 4		
Overall Mean					3811 ± 11			3824 ± 9

Calculated from first arrival travel times on shots at distances greater than 600 m and distances greater than 1000 m. E and W denote shot points to the grid east and grid west of the recording spread, respectively; n is the number of travel time points used in each velocity determination.

The substantial differences in velocities in the two directions at stations BC and RI probably result from sloping iso-velocity surfaces. How large a dip would be required depends strongly on the details of the geometry. For example, if one takes as an approximation a two-layered system comprising a layer of constant velocity equal to 3000 m s⁻¹ (the mean velocity above 100 m) overlying a sloping refractor with velocity equal to v_{\max} , a dip of about half a degree is indicated. If, on the other hand, one imagines an uppermost layer of surficial snow with a dipping base, a dip only one tenth as large, i.e., 1 m per kilometer, would be needed.

Turning to method 2, numerous individual seismograms were recorded at distances greater than 600 m; a least squares cross-spread velocity was calculated for each. The results are presented in Table 4. The average $(v_p)_{\max}$ from 30 stations is 3804 ± 6 m s⁻¹. To test for a dependence of $(v_p)_{\max}$ on x_{\min} , we have taken means separately for $x_{\min} < 1$ km and $x_{\min} > 1$ km at the four stations (BC, H12, I105, and RI) where there were shots in both ranges of x_{\min} . The average $(v_p)_{\max}$ for those four stations for $x_{\min} < 1$ km is 3814 ± 5 m s⁻¹ whereas for $x_{\min} > 1$ km it is 3819 ± 21 m s⁻¹. Clearly the difference is not significant. The possibility of a dependence of $(v_p)_{\max}$ on ice thickness also was examined. The average value of $(v_p)_{\max}$ at the 16 stations where the ice thickness is greater than 500 m is 3812 ± 9 m s⁻¹, whereas at the 14 stations where the ice thickness is less than 500 m it is 3796 ± 7 m s⁻¹, again not a significant difference. There is no prominent pattern in the regional distribution of maximum P wave velocities.

Method 3, measuring v_{\max} by means of multiple surface reflections, is possible only when several clear surface-reflected waves are recorded at a large shot-spread distance. A seismogram from station H12 containing good surface multiples is reproduced in Figure 6, and an illustrative drawing of surface multiples is shown in Figure 7. Let P_n be the arrival time of the multiple that has been reflected n-1 times at the surface, and let δ_{n-1} be the time difference between P_n and P_{n-1} . For any n such that x/n is greater than the minimum distance for the ray path to reach the velocity maximum, $\delta_{n-1} = \delta_{n-2} = \dots = \delta_1$ is the time intercept of the maximum velocity travel time line, and all the P_n are points on that line [Bentley et al., 1957; Bentley, 1964]. This analytical scheme follows directly from the basic seismic refraction principle that intercept time is equal to the difference between the actual travel time of a wave and the time that would be needed for the wave to

TABLE 4. Values of $(v_p)_{\max}$ from Cross-Spread Velocities

<u>Station</u>	<u>n</u>	Minimum Distance, m	Maximum Distance, m	$(v_p)_{\max},$ m s^{-1}
BC	11	892	1233	3789 N
	12	658	1000	3806 W
	12	1158	1500	3762 W
	16	751	1370	3815 W
	13	1658	2340	3765 W
	10	689	1309	3763 W
	14	621	1056	3832 E
	23	629	1342	3822 E
Mean (BC)				3794 \pm 10
G5	14	608	1087	3861
	14	613	1087	3892
	Mean (G5)			
G6 H7 H8 H11S	16	692	1375	3760
	8	783	1096	3816
	21	724	1399	3767
	11	853	1197	3816
H12	14	608	1070	3812
	24	600	1370	3822
	24	900	1670	3840
	24	1200	1970	3838
	24	1500	2270	3847
	24	2000	2770	3850
	Mean (H12)			
I8	22	738	1442	3824
I10S	20	613	1313	3809
	12	1023	1786	3834
	10	1583	2284	3807
	10	2679	3380	3820
	7	3818	4396	3755
	Mean (I10S)			
J7S	11	748	1029	3840
J9DS	13	625	1339	3780
J10	22	656	1412	3808
K3	14	609	1077	3768
K4	21	624	1305	3825
K5	13	610	1135	3771
L5	21	706	1450	3782
M2	23	774	1518	3863
M3	16	611	1105	3791
M5	17	616	1141	3811
M8	16	606	1134	3804
M9	22	630	1310	3785
M10	24	623	1366	3751
N7	23	665	1408	3852
N8	22	738	1480	3822

TABLE 4. (continued)

Station	n	Minimum Distance, m	Maximum Distance, m	$(v_p)_{\max}$, m s ⁻¹
05	18	601	1189	3830
06	22	601	1282	3771
07	17	775	1518	3773
08	12	684	1023	3758
09	12	952	1296	3813
RI	21	627	1269	3799 W
	24	1135	1869	3857 W
	24	4135	4869	3885 W
	24	1131	1865	3816 E
	14	4162	4865	3870 E
	24	640	1364	3841 S
Mean (RI)				3845 ± 13
Overall mean				3804 ± 6

Values of $(v_p)_{\max}$ calculated from cross-spread velocities on individual shots at distances greater than 600 m; n is the number of travel time points on each shot. The standard errors of the individual cross-spread values of $(v_p)_{\max}$ were all $< \pm 5$ m s⁻¹. Symbols N, E, S, and W after velocities at stations BC and RI indicate shots grid north, east, south, and west, respectively, of the recording spread.

move in a straight line from shot to detector at the highest velocity encountered along the refraction path [Dobrin, 1960]. The results of the analyses of surface multiples are listed in Table 5. The average $(v_p)_{\max}$ for four stations is 3828 ± 9 m s⁻¹. Note that the difference between velocities shot in opposite directions at BC and RI, previously attributed to sloping iso-velocity planes, again appears. That implies that the slope, if it is real, must extend to the full length of the profile: 2 km at BC and 5 km at RI.

The average $(v_p)_{\max}$ as calculated by methods 1, 2, and 3, 3811 ± 7 , may be compared with other values from refraction shooting on ice shelves: 3810 m s⁻¹ at Ellsworth Station on the Filchner Ice Shelf [Thiel and Behrendt, 1959], 3810 m s⁻¹ at Maudheim [Robin, 1958], and 3789 ± 7 m s⁻¹ on the Ross Ice Shelf (Crary et al. [1962a]; average of 18 measurements in their Table 7). All these values of $(v_p)_{\max}$ are substantially lower than those commonly found on grounded ice sheets. (Thiel and Ostenso [1961] obtained a larger value (3839 m s⁻¹ between 85 m and 110 m in depth) using a downhole geophone in a borehole at Little America V, but the difference is statistically not significant. They make no determination of error limits, but an uncertainty in travel time of 0.5 ms, such as we estimate for our work, would have produced a 300 m s⁻¹ uncertainty in velocity over the 25-m interval.) Kohnen [1974] presents a

compilation from various investigators of 31 values of wave speeds in grounded ice: they ranged from 3836 to 3950 m s⁻¹, depending on temperature, with a velocity of 3850 m s⁻¹ corresponding to -24°C, the measured temperature at 80-m depth in the drill hole at station J9DC [Clough and Hansen, 1979]. (Station J9DC is the station where the RISP drilling actually took place in 1976-1978; it is about 2 km from the preselected site, J9DS.) This discrepancy between ice shelves and the grounded ice sheet has been noted previously by Thiel and Ostenso [1961] and Bentley [1964] and has been attributed variously to differences in density structure, temperature structure, and crystal orientation between ice shelves and grounded ice sheets [Thiel and Ostenso, 1961], but no quantitatively satisfactory explanation yet exists.

Ultrasonic velocity measurements on core samples from the Ross Ice Shelf and sonic velocity logging in the RISP drill hole at station J9DC might be expected to shed light on the matter, but they fail to do so. The logging yielded minimum velocities slightly less than 3800 m s⁻¹ [Bentley and Jezek, 1981], consistent with the refraction results, whereas the ultrasonic measurements gave velocities comparable to, or higher than, those on grounded ice [Bennett, 1972; Kohnen and Bentley, 1977], except after the ice had relaxed, leading to the formation of microcracks [Kohnen and Gow, 1979]. The

RIGGS I
 STATION: H12
 DATE: 24 JAN 74
 RECORD: 14
 CHARGE: 0.15 kg
 DEPTH: 4 m
 SHOT LOCATION:
 1.2 km from 1
 TAKEOUTS: 31 m
 FILTERS:
 LOW: 210 hz
 HIGH: none
 ATTENUATION:
 1-12: 10 db
 13-24: 0

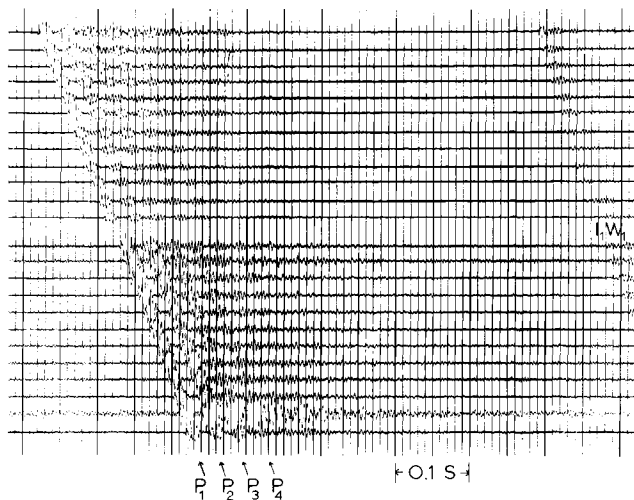


Fig. 6. Seismogram from station H12 illustrating P waves multiply reflected from the surface (P_n).

observed fabrics (roughly a 25° - 30° surface cone [see Kohnen and Gow, 1979]) should not lead to an appreciable lowering of the wave velocity according to the curves given by Bennett [1972].

Primarily because of the difficulty in generating S waves, $(v_s)_{\max}$ was poorly determined during RIGGS I and II. The only determination was at station BC, where the least squares inverse slope of six arrivals between 813 and 2090 m is $1970 \pm 44 \text{ m s}^{-1}$. This can be compared with 1978 m s^{-1} obtained at Little America V through borehole logging (Thiel and Ostenso, [1961]; no error cited) and to 12 values for grounded ice sheets ranging from 1934 to 1960 m s^{-1} , averaging $1945 \pm 8 \text{ m s}^{-1}$, tabulated by Kohnen [1974] from his work and that of Bentley et al. [1957] in Greenland and Bentley [1971] in Antarctica.

Average Compressional Wave Velocity

The average P wave velocity, \bar{v}_p , through the whole ice shelf may be calculated by the oblique reflection technique if reflections from the ice-water interface (called I_1 reflections after the notation of Crary et al. [1962a]) are received over a reasonable interval of distance on one or more seismograms at a station. Enough good I_1 reflections (or doubly reflected I_2 arrivals in the case of station Q5) to determine \bar{v}_p were recorded on ten profiles at nine stations during RIGGS I and II. A determination on each of two perpendicular profiles was possible at station Q5. A typical seismogram is reproduced in Figure 8. Recordings were made at paper speeds of about 300 mm s^{-1} , and travel times have been picked to the nearest

millisecond with an estimated uncertainty of ± 2 ms. Low-cut filtering in the 100- to 300-Hz range and high amplifier gain were found to produce the clearest reflected signals and were used generally in recording. Charge sizes ranged from $1/3$ to 5 lb (0.15 to 2.3 kg) of Dupont HDP primers or Seismogel; shot holes were 4 or 5 m deep. Reflection times have been corrected for uphole travel, and average velocities have been obtained by least squares fitting of regression lines to graphs of travel time squared, t^2 , versus x^2 (Table 6).

Ice thickness was measured by radar along the seismic lines at three of the stations. At those stations, \bar{v}_p has been corrected for the slope of the ice-water interface according to the formula

$$\bar{v}_p^2 t_2 = x^2 + 4h_i^2 + 4h_i x \sin \beta$$

where h_i is the ice thickness and β is the slope of the ice-water interface relative to the surface, positive when the ice thickens with increasing x .

One should find that \bar{v}_p increases as ice thickness increases, since the thicker the ice, the less the proportion of the wave path

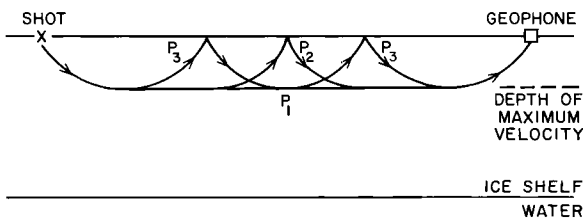


Fig. 7. Schematic diagram of P_n waves.

TABLE 5. Values of $(v_p)_{\max}$ Calculated From Multiple Surface Reflections

<u>Station</u>	<u>Shot Location</u>	<u>Shot No.</u>	<u>Trace</u>	<u>Shot Distance, m</u>	<u>Multiples Used</u>	$(v_p)_{\max}, \text{m s}^{-1}$	<u>Average</u>
BC	W	31	4	1751	P_1, P_2	3774 ± 1	
			5	1782		3799 ± 1	
			8	1875		3774 ± 1	3782 ± 14
			22	1292		3828 ± 1	
	E	74	23	1322		3830 ± 1	
			24	1352		3842 ± 1	3833 ± 8
							3808 ± 11
	Mean (BC)						
	H12	14	15	1689	P_1, P_2, P_3	3824 ± 2	
			16	1721		3838 ± 7	
			17	1752		3819 ± 5	
			20	1846		3821 ± 1	3824 ± 5
Mean (H12)							3824 ± 5
I10S	W	10	20	1662	P_1, P_2, P_3	3806 ± 2	
			22	1724		3796 ± 4	3801 ± 7
Mean (I10S)							3801 ± 7
RI	W	B20	1	4135	P_1, P_2, P_3, P_4	3894 ± 4	
			2	4166		3891 ± 1	
			4	4227		3879 ± 1	
			5	4257		3877 ± 1	
			6	4288		3882 ± 1	3885 ± 7
	E	B50	19	4712	P_1, P_2, P_3, P_4	3818 ± 1	
			20	4743		3819 ± 1	
			21	4773		3823 ± 1	
			22	4804		3824 ± 1	
			24	4865		3821 ± 1	3821 ± 3
	Mean (RI)						3853 ± 6
Overall mean							3828 ± 9

Symbols E and W denote shots grid east and grid west, respectively, of the recording spread.

in low-velocity firn. However, when \bar{v}_p is plotted against ice thickness (Figure 5) together with a theoretical curve calculated using the data in Table 2 and the assumption that \bar{v}_p decreases linearly from 3811 m s^{-1} at 100 m to 3770 m s^{-1} at the ice-water interface owing to increasing ice temperature, it becomes clear that the expected effect is too small to be seen. The mean value from the RIGGS stations, $3688 \pm 15 \text{ m s}^{-1}$, agrees well with the theoretical curve. This indicates that there is no broadly consistent effect of anisotropy in the ice.

Density and Elastic Moduli

Calculation of the variation of the elastic moduli between the surface of the ice shelf and the depth of maximum seismic velocity is possible when v_p , v_s , and density ρ all are known as functions of depth.

Lacking direct measurements of ρ , one may calculate it from the semiempirical equation of Kohnen [1972]:

$$\rho(z) = \frac{0.915 \text{ Mg m}^{-3}}{1 + \left[\frac{(v_p)_{\max} - v_p(z)}{2250} \right]^{1.22}} \quad (2)$$

0.915 Mg m^{-3} is the approximate density of bubbly glacier ice at the depth of $(v_p)_{\max}$. We have set $(v_p)_{\max} = 3850 \text{ m s}^{-1}$, the expected value at a temperature of -24°C . During RIGGS II a hole was drilled to a depth of 100 m at station J9DS. Densities measured on segments of the recovered core [Langway, 1975] are compared in Figure 10 with seismically computed densities. The good agreement supports the use of Kohnen's equation for other locations where no drill holes are available.

RIGGS I
 STATION: I7
 DATE: 31 DEC 73
 RECORD: 5
 CHARGE: 1.1 kg
 DEPTH: 4 m
 SHOT LOCATION:
 10 m from 1
 TAKEOUTS: 31 m
 FILTERS:
 LOW: 120 Hz
 HIGH: none
 ATTENUATION:
 1-24: 0

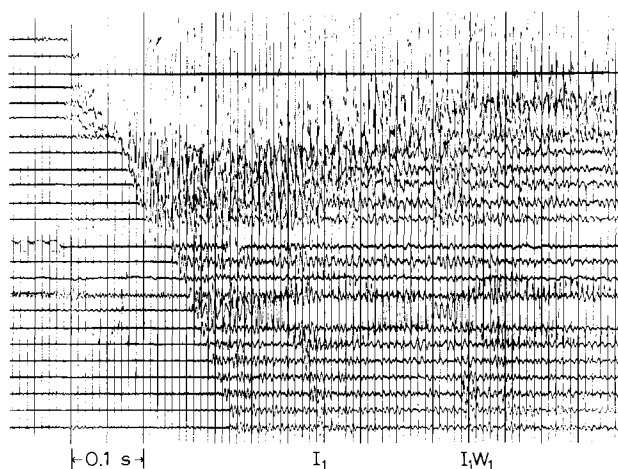


Fig. 8. Seismogram from station I7 illustrating the ice bottom (I_1) and ocean bottom (I_1W_1) reflections.

The use of $(v_p)_{\max} = 3850 \text{ m s}^{-1}$ implies that a glacier ice density of 0.915 Mg m^{-3} (Kohnen [1972], discusses this choice of density) corresponds to that velocity, whereas $(v_p)_{\max}$ in the ice shelf was only 3811 m s^{-1} and the measured maximum density in the ice shelf, at Little America V, is only 0.915 Mg m^{-3} . The density difference that would result from using 3811 m s^{-1} and 0.912 Mg m^{-3} in equation (2) rather than 3850 m s^{-1} and 0.912 Mg m^{-3} is within 10% of 0.007 Mg m^{-3} for depths of 25 m and greater (less at lesser depths). That is not enough to affect significantly the agreement between measured and calculated densities shown in Figure 10.

Densities and elastic moduli computed at the RIGGS short-refraction sites are tabu-

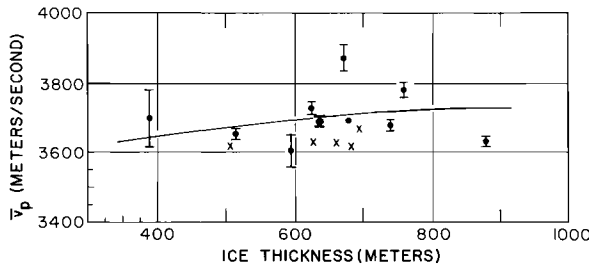


Fig. 9. Mean P wave velocity through the ice shelf, \bar{v}_p , versus ice thickness. Solid dots with error bars are RIGGS data; crosses denote values from Crary et al. [1962a]. The continuous line is a theoretical relationship based on measured and inferred v_p in the shelf. The large solid circle with error bars is the average from the RIGGS stations.

lated in Appendix B2 (microfiche). Average densities computed from the averaged v_p versus z data are included in Table 2. The elastic moduli are plotted in Figures 11 to 15 as functions of density, since density is a more fundamental property than depth.

Poisson's ratio (Figure 11) displays a large amount of scatter at the lower densities, which probably reflects both the complex texture of partially compacted, granular, near-surface firn and the

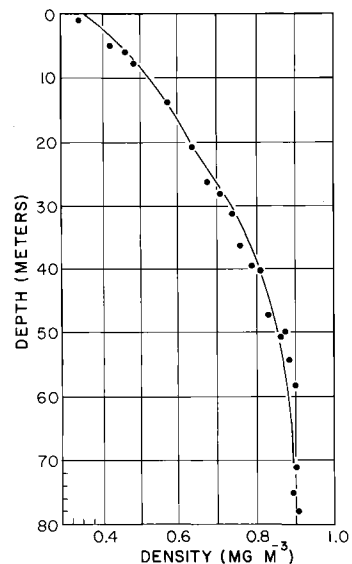


Fig. 10. Density versus depth at station J9DS, as measured on ice cores (points) and computed from v_p by equation (2) (solid line).

TABLE 6. \bar{v}_p Determined From Oblique Reflections

Station	Shot No.	Ice Thickness, m	n	Minimum Distance, m	Maximum Distance, m	Slope of Ice-Water Interface, deg	Slope Correction, $m s^{-1}$	Corrected \bar{v}_p , $m s^{-1}$
E8	1	830	22	41	804	+1.4	+35	3638 ± 12
F9	2	640	24	10	803			3693 ± 7
H11S	3, 4, 5	600	24	10	947	+0.4	+11	3733 ± 18
I7	3	510	10	459	798			3653 ± 15
K3	4	760	8	363	1015			3781 ± 22
L5	4	730	13	706	1451			3680 ± 16
M2	2	670	9	774	1113			3869 ± 39
N6	3	580	7	334	1048			3599 ± 51
Q5-1	2	400	11	31	339	+1.1	+18	3746 ± 130
Q5-2	2	400	6	62	374	+1.3	+18	3669 ± 101
Mean								3688 ± 15

There are $n t^2 x^2$ points on each profile. The slope of the ice-water interface was determined by radar at stations E8, H11S, and Q5. The listed value of \bar{v}_p for those stations includes the slope correction. The other values of \bar{v}_p are uncorrected. Profiles 1 and 2 at station Q5 were laid out nearly normal to each other.

difficulty of measuring seismic velocity accurately within a few meters of the surface. A summary of Poisson's ratio for dry snow by Mellor [1964] shows similar scatter. The remaining elastic moduli are reasonably regular functions of density. On the graph of Young's modulus (Figure 12) and, to a lesser extent, on the others, there is a clear suggestion of an increase at $\rho \approx 0.55 \text{ Mg m}^{-3}$ in the rate of change of modulus with density that probably reflects a change in densification mechanism (see next section). According to a review paper by Roethlisberger [1972], the most accurate values of the elastic moduli of idealized, nonporous, isotropic, polycrystalline ice are those computed by Brockamp and Querfurth [1964] and by Bennett [1968] from experimental data on elastic wave velocities in single ice crystals. Values so computed (plotted in Figures 11 to 15) are consistent with the trends of the data obtained from our short-refraction profiles.

Densification Horizons Derived from Seismic Velocity Gradients

Exponential functions of the form

$$\frac{dv_p}{dz} = (dv_p/dz)_o e^{-\gamma z} \quad (3)$$

where $(dv_p/dz)_o$ and γ are constants, have been used successfully to approximate seg-

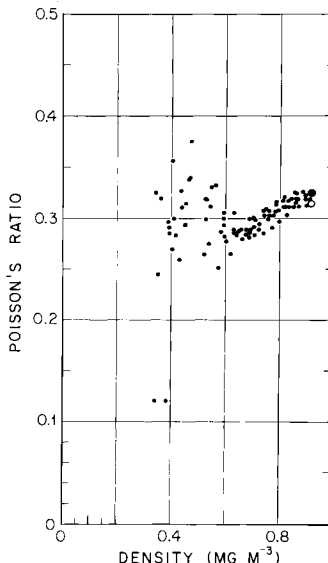


Fig. 11. Poisson's ratio versus density. RIGGS measurements are denoted by dots. Values of Poisson's ratio for solid ice from Brockamp and Querfurth [1964] and Bennett [1968] are denoted by an open circle and a solid circle, respectively.

ments of curves of the vertical gradient of v_p on the ice sheets of Greenland [Brockamp and Pistor, 1967] and Antarctica [Kohnen and Bentley, 1973; Robertson and Bentley, 1975]. Kohnen and Bentley [1973] correlated the depths at which the constants change at old and new Byrd stations with significant changes in the densification process of the firn. Robertson and Bentley [1975] analyzed 50 Antarctic profiles and found that 43 could be fit satisfactorily in sections by equation (3). Results from RIGGS short-refraction data are tabulated and plotted for individual stations in Appendix B3 (microfiche). Mean values and standard deviations of the velocity gradients are plotted in Figure 16.

Kohnen and Bentley [1973] and Robertson and Bentley [1975] identified one change in slope (called "B" by Robertson and Bentley [1975]) that appears to correlate with the "critical depth" of Anderson and Benson [1963]. Anderson and Benson [1963] explained the "critical depth" as the limit of "close random packing" below which grain packing is no longer an effective densification mechanism. However, Gow [1968] found that intergrain bonding is too well developed even at shallow depths to permit simple mechanical rearrangement of grains. Alley [1987a] has presented a theory that quantitatively explains densification at low densities by viscous grain boundary sliding; boundary "B" then corresponds to the depth below which power law creep dominates over grain boundary sliding.

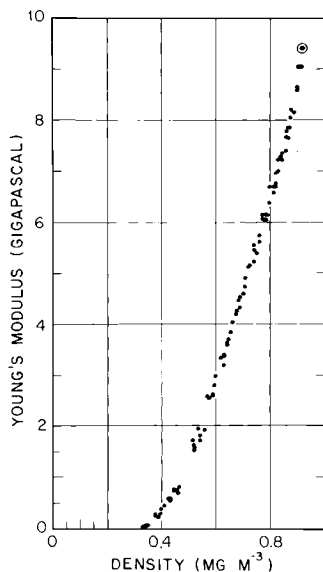


Fig. 12. Young's modulus versus density. RIGGS measurements are denoted by dots. The value for solid ice from both Brockamp and Querfurth [1964] and Bennett [1968] is denoted by concentric open and solid circles.

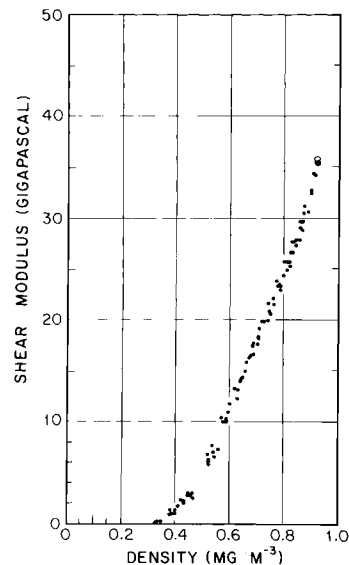


Fig. 13. Shear modulus versus density. RIGGS measurements are denoted by dots. Values for solid ice from Brockamp and Querfurth [1964] and Bennett [1968] are denoted by an open circle and a solid circle, respectively.

Another slope change ("D") correlates with the depth at which the firn becomes impermeable, by definition the firn-ice boundary. Robertson and Bentley [1975] identified a third break ("C") between B and D at stations where the mean annual accumulation is relatively high and suggested several possible explanations.

Depths to B, C, and D at RIGGS short-refraction stations are listed in Table 7. Mean depths to the horizons are 11 ± 2 m, 25 ± 10 m, and 46 ± 8 m, respectively. The first two values agree reasonably well with values of 9 ± 2 m and 28 ± 4 m for B and C calculated for the West Antarctic stations by Robertson and Bentley [1975].

Though it appears on three individual profiles (two at station BC and one at station H1S), C does not show up in the trend of the mean values of the RIGGS velocity gradients (Figure 16). This is expected from the previous finding that C tends to appear only where mean annual snow accumulation is relatively high. The annual accumulation generally is less than 100 mm of water in the grid western portion of the Ross Ice Shelf except near the ice front or the Transantarctic Mountains [Clausen et al., 1979]. The parameters of the least squares lines through the RIGGS mean values are $(dv_p/dz)_o = 283 \pm 17 \text{ s}^{-1}$, $\gamma = 110 \pm 9 \text{ km}^{-1}$ for the segment A-B; $(dv_p/dz)_o = 97 \pm 4 \text{ s}^{-1}$,

TABLE 7. Depths to Breaks in Plots of $\ln v_p/dx$ Versus z From Short-Refraction Profiles

Station	B, m	C, m	D, m	b_o , mm yr^{-1}	T, $^{\circ}\text{C}$
BC-A	9	20	39	81	-27.6
BC-B	10	18	47	81	-27.6
H7	13		35	74	-27.8
H11S	11	36	55	118 (from H11)	-24.5*
I10S	12			62 (from I10)	-24.9*
J7S			44	75 (from J6)	-28.5 (from J6)
J9DS	14			90	-27.6 (from J9)
K11	8			100	-26.4†
P5	11			230	-24.5*
RI	13		54	121	-27.5
Mean	11 ± 2	25 ± 10	46 ± 8		

*Interpolated.

†Measured at 8-m depth instead of 10 m.

Blank spaces indicate that no distinct break was discernible (cf. Appendix B3). Accumulation rates (b_o) are from Clausen et al. [1979] except at P15; (b_o) there and all 10-m temperature values (T) are from Thomas et al. [1984]. Data from neighboring stations are indicated.

$\gamma = 34 \pm 1 \text{ km}^{-1}$ for the segment B-D; and $(dv_p/dx)_o = 1300 \pm 900 \text{ s}^{-1}$, $\gamma = 90 \pm 9 \text{ km}^{-1}$ for the segment D-end. There is good agreement between the mean velocity gradient curve from this work and that for low accumulation rates from Robertson and Bentley [1975] (Figure 16).

Anisotropy

Naturally occurring single crystals of ice belong to the hexagonal crystallographic system; so their elastic properties are transversely isotropic with respect to the c axis (optic axis). When crystals are combined to form a polycrystalline mass such as an ice sheet, any nonrandom arrangement of the c axes produces directionally dependent seismic properties. Seismic velocity measurements on single ice crystals (see Roethlisberger, [1972], for a review) show that v_p can vary by as much as 5% as a function of the direction of wave propagation; the highest speed is parallel to the c axis. Variations are even greater for S waves: up to 18% for waves polarized in a plane containing the c axis. Evidence for seismic anisotropy in the Antarctic ice sheet has been presented by Bentley [1964, 1971] from refraction shooting; by Clough and Bentley [1970] from comparison between seismic and radar echo times; by Thiel and

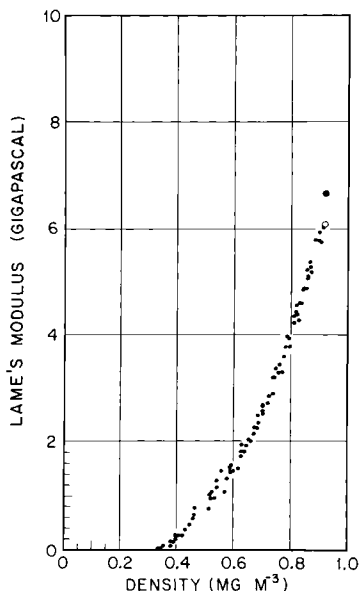


Fig. 14. Lamé's modulus versus density. RIGGS measurements are denoted by dots. Values for solid ice from Brockamp and Querfurth [1964] and Bennett [1968] are denoted by an open circle and a solid circle, respectively.

Ostenso [1961], Bentley [1972], and Bentley and Jezek [1981] from sonic logging in drill holes at Little America V, Byrd Station, and RIGGS station J9DS; and by Kohnen and Bentley [1977] and Kohnen and Gow [1979] from ultrasonic velocity measurements on ice cores from J9DS and Byrd Station, respectively. Core samples from the drill holes revealed a pronounced vertical (single-pole) orientation of c axes between the depths of 900 and 1800 m at Byrd Station [Gow, 1970a; Gow and Williamson, 1976] and various multipolar patterns of concentration at angles of 20° to 40° from the vertical, at depths between 65 m and the bottom of the ice shelf at Little America V [Gow, 1963, 1970b].

A different type of anisotropy was reported by Bennett [1968, 1972], who found from ultrasonic measurements on near-surface snow at Byrd Station that v_p is up to 1.5 times greater vertically than horizontally within a few meters of the surface. Some difference persists to a depth of about 30 m. Bennett [1968, 1972] attributed this effect to an unexplained "structural anisotropy." We believe it probably results from the textural anisotropy found by Alley [1987b] at another West Antarctic site: elongate grains preferentially bonded near their ends into vertical columns.

For seismic shooting on an anisotropic medium it is necessary to distinguish between

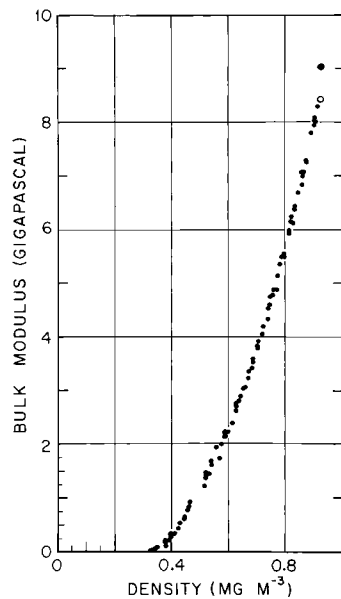


Fig. 15. Bulk modulus versus density. RIGGS measurements are denoted by dots. Values for solid ice from Brockamp and Querfurth [1964] and Bennett [1968] are denoted by an open circle and a solid circle, respectively.

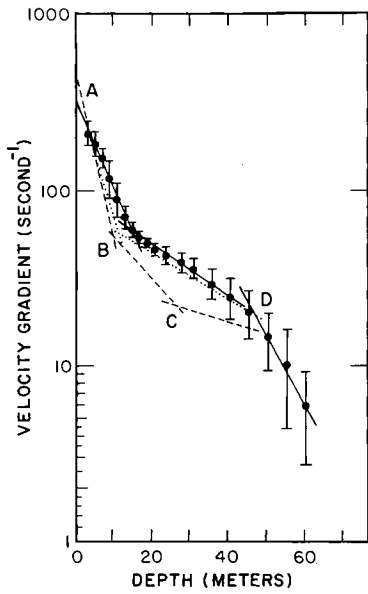


Fig. 16. Mean dv_p/dz versus depth for 10 short-refraction profiles from RIGGS I and II. Solid dots denote the RIGGS values; error bars denote the standard errors in the means. The dotted and dashed lines are mean curves from Robertson and Bentley [1975] for low (-100 ± 50 mm water per year) and high (-270 ± 100 mm water per year) surface accumulation rates, respectively.

v_{sh} , the speed of shear (SH) waves polarized horizontally, and v_{sv} , the speed of shear (SV) waves polarized in the plane of propagation. Evidence bearing on anisotropy in ice shelves from RIGGS I and II consists of (1) a comparison between v_{sv} and v_{sh} from short-refraction profiles at station RI and (2) a comparison between seismic and radar echo times.

Comparison between v_{sv} and v_{sh} . Two S wave short-refraction profiles were recorded along the same line at station RI. On the first, geophones were oriented transversely to the line, and the 4" x 4" stake was hit transversely to record the horizontally polarized SH waves. On the second, geophones were placed longitudinally, and the stake was hit along the line to record the SV waves, which are polarized in the plane of incidence. A schematic diagram is shown in Figure 17, a seismogram illustrating SV arrivals is reproduced in Figure 18, and the resulting velocity-depth curves are plotted in Figure 19.

The estimated error due to uncertainties in travel times is ± 30 m s $^{-1}$ at the surface for both v_{sv} and v_{sh} , diminishing to ± 20 m s $^{-1}$ at 20 m and to ± 10 m s $^{-1}$ at 50 m. This

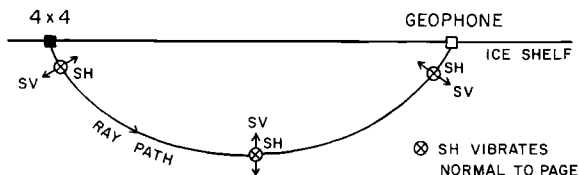


Fig. 17. Polarizations of SV and SH waves along a ray path in polar firn. SV waves are polarized as shown by arrows; SH waves are polarized normal to the page.

does not take into account errors in depth that arise from applying equation (1) to an anisotropic medium [Bennett, 1968, 1972]. Significant differences between v_{sv} and v_{sh} occur in the top few meters of snow, where v_{sv} is higher by up to 40%, and between 10 and 25 m, where it is less by as much as 8%. There is also a suggestion that v_{sv} is significantly less than v_{sh} below 55 m, but the data do not extend deep enough to be sure. The anisotropy very near the surface is consistent with Bennett's [1968, 1972] observations and Alley's [1987b] description of the firn as being bonded more strongly vertically than horizontally (see the discussion by Kirchner and Bentley [this volume]). The indicated higher v_{sh} at intermediate depths is unexpected and could result from errors associated with equation (1). If the difference is real, possible explanations include (1) some kind of anisotropy in the structure of the firn owing to high longitudinal strain rates in the ice shelf and (2) an abundance of horizontal ice lenses between 10 and 25 m.

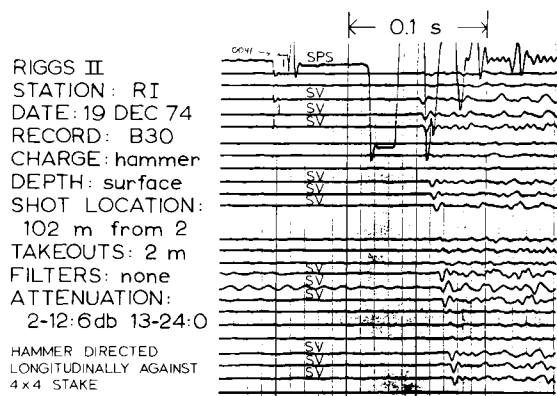


Fig. 18. Seismogram from station RI illustrating SV waves. "SPS" stands for shot-point seismometer, i.e., a geophone placed against the 4" x 4" stake.

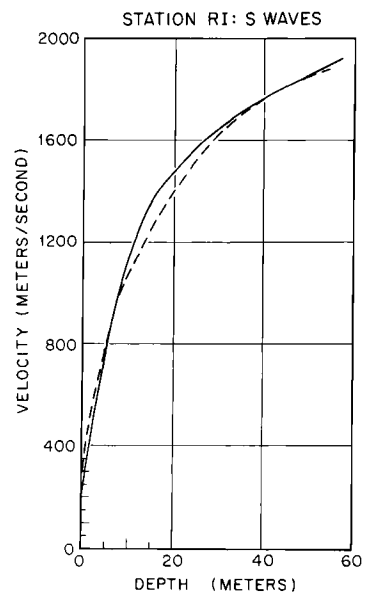


Fig. 19. S wave velocities versus depth at station RI. Solid line is v_{sh} ; dashed line is v_{sv} .

Seismic versus radar echo times. Although seismic anisotropy can reach 5%, anisotropy in the electromagnetic wave speed at radar sounding frequencies is less than 0.5% [Johari and Jones, 1978]. Comparison of seismic and radar echo times from the same interface should, therefore, be a measure of anisotropy through variations in v_p . The wavelengths of electromagnetic and seismic waves in ice are not greatly different: about 5 m at 35 MHz and 20 m at 200 Hz, respectively. To make the comparison, we have plotted $\Delta h_i = h_i(\text{radar}) - h_i(\text{seismic})$ versus ice thickness h_i computed from spot radar soundings at the various stations (Figure 20; see Table 8 for actual values). The estimated error in measuring either the seismic or the radar travel time is ± 10 m; so the estimated error in a single measurement of Δh_i is ± 14 m.

It is clear from Figure 20 that there is no significant correlation between Δh_i and h_i (the correlation coefficient is only 0.2). The mean value of Δh_i is -2.3 m with standard errors of 15.0 m for an individual value and 2.2 m for the mean. The individual standard error is essentially the same as estimated a priori on the basis of errors in time measurement, and the mean is not significantly different from zero. We conclude, therefore, that there is no indication of an overall systematic difference, such as could arise from anisotropy or different effective

reflection surfaces for seismic and electromagnetic waves.

At one station, I10S, Δh_i is particularly large and negative. This might be a statistical fluctuation, but it may be significant that I10S is on Crary Ice Rise. Where ice rests directly on soft, wet sediments, the acoustic impedance contrast at the boundary may be very low (as discussed further below). Thus it is possible that the seismic reflection recorded at I10S comes not from the base of the ice, but from a deeper horizon in the sedimentary column. Assuming $v_p = 1700 \text{ m s}^{-1}$ in the uppermost sediments leads to a seismic reflector depth of 20 m below the base of the ice. It is interesting to note that on the largest ice rise in the Ross Ice Shelf, Roosevelt Island, Δh is also large (60 m) but positive rather than negative, a circumstance that is much more difficult to explain. Only a special kind of sediment just below the ice would yield a dielectric contrast low enough to allow an explanation by penetration of the electromagnetic wave combined with reflection of seismic wave [Jiracek, 1967; Jiracek and Bentley, 1971].

If we neglect station I10S, there is, surprisingly, a difference between the mean values of Δh_i from the two seasons that is statistically significant at the 99% confidence level: $10.2 \pm 4.0 \text{ m}$, or about 2% of the mean ice thickness. The individual season means are $4.2 \pm 3.2 \text{ m}$ for RIGGS I and $-6.0 \pm 2.4 \text{ m}$ for RIGGS II; the latter also is significantly different from zero at the same level. Seismic and radar instrumentation was the same in both seasons, and timing was carefully checked; so there is no possibility of a 2% clock error in either kind of equipment. A possible physical explanation is that at many of the RIGGS II sites there has been a freezing on of a layer of sea ice of the order of 10 m thick. However, this does not accord well with the distribution of melting and freezing zones delineated by Neal [1979] from the analysis of radar echo amplitudes. Furthermore, no clear regional pattern is evident in the geographical distribution of Δh_i . Thus we have no firm explanation for the difference.

Ice Thickness and Sea Bottom Topography

Survey Results

The thickness of the ice shelf and the depth to the sea bottom beneath the shelf may be calculated from travel times of radar and seismic reflections when the electromagnetic and seismic wave speeds are known. Seismic wave speeds in the ice are derived from short-refraction profiling, maximum velocity calculations, and t^2 versus x^2 analyses as

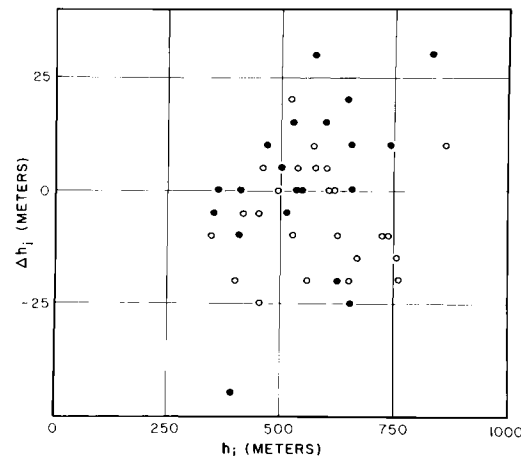


Fig. 20. Plot of $\Delta h_i = h_i(\text{radar}) - h_i$ (seismic) versus h_i (radar). Solid circles are data from RIGGS I; open circles are from RIGGS II.

discussed in the preceding section. Radar reflection times in microseconds (t_r) were converted to ice thicknesses in meters (h_i) using the relation $h_i = 84.3t_r + 7.6$. The wave speed was taken from the accurate measurement by Robin [1975], and the additive constant was calculated from the excess thickness of the ice that is represented by the air in the firn [Shabtaie and Bentley, 1982] and the relationship between density and wave speed of Robin et al. [1969]. A constant value of 1.44 km s^{-1} is appropriate for the acoustic wave speed in seawater beneath the shelf [Crary et al., 1962a]. Radar sounding normally produces a clear, high-amplitude echo from the ice-water interface, but none deeper. The seismic technique, on the other hand, usually produces a recognizable ocean bottom echo, whereas the ice bottom echo often is lost in the noise of surface multiple and direct shear wave arrivals. The combination of the two methods thus is highly effective in determining both the ice thickness and the water depth.

Multiple seismic echoes were recorded at about 20% of the survey sites. A multiple is an arrival that has been reflected more than once off an interface (Figure 21); a particularly good example is shown in Figure 22. Multiples are useful in that various combinations of their arrival times often yield the arrival time of a fundamental reflection (for example, $I_2W_1 - I_1W_1 = I_1$) when the fundamental reflection itself is hidden in surface noise. I_1W_1 is virtually always present (if the ice is afloat) as the

TABLE 8. Ice Thicknesses (h_i), Water Layer Thicknesses (h_w), Depths to the Seafloor, and $\Delta h_i = h_i(\text{Radar}) - h_i(\text{Seismic})$

<u>Station</u>	<u>$h_i(\text{Radar})$, m</u>	<u>$h_i(\text{Seismic})$, m</u>	<u>Δh_i, m</u>	<u>h_w, m</u>	<u>Depth to the Seafloor, m Below Sea Level</u>
BC	480	NR		143	557
E5	783	NR		0	639
E6	733	NR		0	588
E7	834	NR		0	712
E8	859	828	31	189	940
F7	749	738	11	0	633
F9	665	643	22	159	737
G4	657	657	0	0	481
G5	556	NR		(0)	401
G6	606	577	33	0	477
G8	665	655	10	89	667
H5	631	653	-22	41	590
H6	657	NR		0	529
H7	505	499	6	21	456
H8	539	NR		30	496
H9	606	627	-21	72	597
H10	547	529	18	50	523
H11S	615	602	13	125	658
H12	412	411	1	461	803
I5	530	530	0	0	417
I6	547	545	2	85	558
I7	505	509	-4	152	587
I8	471	NR		105	510
I9	463	NR		150	548
I10S	345	389	-44	0	242
I11	488	NR		144	564
IJ9%	395	NR		211	548
J4	876	863	13	0	285
J6	539	533	6	21	487
J7S	480	470	10	41	454
J8	471	NR		159	564
J9	421	NR		236	596
J9DS	412	NR		244	596
J10	320	NR		296	566
JK9%	395	403	-8	326	664
K3	741	755	-14	66	712
K4	741	NR		158	804
K5	480	NR		64	477
K7	588	NR		53	473
K9	421	NR		199	559
K10	362	359	3	414	722
K11	345	348	-3	309	601
L4	716	725	-9	73	697
L5	724	734	-10	42	673
L6	682	NR		51	644
L7	539	NR		13	479
L9	370	NR		170	485
L11	370	NR		282	597
M2	657	672	-15	58	629
M3	741	762	-21	98	744

TABLE 8. (continued)

Station	h_i (Radar), m	h_i (Seismic), m	Δh_i , m	h_w , m	Depth to the Seafloor, m Below Sea Level
M5	623	NR		96	637
M6	606	606	0	109	634
M6½	615	625	-10	71	604
M7	581	NR		135	638
M8	480	NR		202	615
M9	446	449	-3	78	461
M10	370	NR		64	379
N4	631	651	-20	209	757
N5	539	558	-19	222	688
N6	581	576	5	218	721
N7	606	601	5	176	701
N8	522	NR		215	665
N9	370	NR		197	512
N10	387	NR		54	384
O4	513	525	-12	216	658
O5	581	571	10	211	714
O6	539	522	17	317	783
O7	320	NR		133	403
O8	463	462	1	186	584
O9	412	413	-1	190	542
OP4	497	495	2	0	113
P5	429	453	-24	198	565
P6	446	449	-3	304	687
Q5	379	398	-19	258	580
Q6	336	344	-8	396	680
RI	615	616	-1	152	685

NR, no I_1 reflection or multiples yielding I_1 . Parentheses mean value is assumed.

strongest echo on the record. I_2W_1 can be distinguished from I_1W_2 by reasonableness of indicated ice and water layer thicknesses. I_1 arrives too early to be anything else. Usually the ice thickness is known independently anyway from radar echoes. Only at one or two stations in the entire RIGGS program was there any ambiguity in the interpretation of the multiple echoes.

Values of ice thickness, water thickness, and ocean bottom elevation are listed in Table 8. A more complete tabulation of survey data is in Appendix C (microfiche), including actual radar and seismic travel times, seismogram numbers, shot-geophone distances, methods of computation, use of multiples in calculation, etc. Ice thicknesses are estimated to be accurate to ± 15 m, the standard error in the comparison of radar and seismic echo times. The accuracy of water layer thicknesses is estimated at ± 5 m for the seismic multiple method of computa-

tion and ± 10 m where ice thickness is determined only by radar (these errors are smaller than errors in ice thickness because of the low sound velocity in water). Elevation of the seafloor at floating stations was determined from the ice and water thicknesses by assuming hydrostatic equilibrium of the floating ice to calculate its surface elevation. At grounded stations, bed elevations were computed from ice thicknesses and barometric ties to the base camps. The data on water layer thickness and ocean bottom elevation have been included in the maps presented in the accompanying paper by Albert and Bentley [this volume], and previously in the work of Greischar and Bentley [1980] and Robertson et al. [1982]. The ice thickness values contributed to the ice thickness map published by Bentley et al. [1979], although that map was based primarily on airborne radar sounding.

Reflections recorded at stations E5, E6,

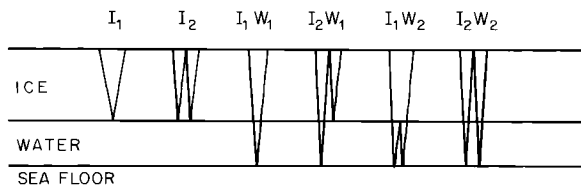


Fig. 21. Ray paths for multiple seismic reflections.

E7, G6, and H6 have been reinterpreted recently in light of the demonstration that the ice cannot be afloat there [Bentley et al., 1987; Shabtaie and Bentley, 1987]. The values in Table 8 and Appendix C (microfiche) reflect that reinterpretation and thus differ from the values given by Robertson [1975].

Sea Bottom Slopes

The local slope of the seafloor at a station can be computed if I_1W_1 reflections are recorded along perpendicular profiles ("L spreads"). Determinations of the local dip and strike of the seafloor have been made at nine sites (Table 9). Dips are all 1° or less.

L spread determinations are important first because bottom slope could be a significant source of error in the calculation of sea bottom elevation by the reflection technique. But for a bottom slope of only 1° (assuming also a flat ice-water interface and a 200-m-thick water layer) and an incident angle of 20° at the water-sediment boundary

(an extreme value), reflection times are changed by no more than 2 ms, even for a spread along the line of maximum dip. This difference corresponds to only a few meters in water depth, which is a negligible uncertainty.

Local slopes also provide some information on bottom irregularity through comparison with regional values. The directions of regional slope for the nine L spread stations have been picked from the map of submarine topography [Albert and Bentley, this volume] and are listed in Table 9. (Slope magnitudes are of the order of a few tenths of a degree; more precise estimates on the basis of the map are not justified.) Six of the nine local strikes are within 30° of the regional strikes. Regional and local dips are on the same side of strike at eight stations. It appears that short-wavelength topography (of the order of a few kilometers) superimposed on long-wavelength topography (tens of kilometers) is uncommon.

Finally, L spreads are useful in estimating the magnitudes of the topographic corrections that should be applied to values of gravity measured on the ice shelf. Owing to the small slopes, the topographic corrections to RIGGS gravity data are minimal.

Subbottom Characteristics

Information on the character of the sediments and bedrock beneath the Ross Ice Shelf was obtained by three seismic methods during RIGGS I and II: (1) determination of interval velocities in the sediments, (2) calculation of sea bottom reflection coefficients and acoustic impedances, and (3) seismic refraction shooting.

Interval Velocity

If seismic reflections are recorded from a sequence of flat, parallel layers, the "interval velocity" in the nth layer, v_n , is given by the equation [e.g., Dix, 1955]

$$v_n^2 = (\bar{v}_{n-1}^2 t_n - \bar{v}_n^2 t_{n-1}) / (t_n - t_{n-1}) \quad (4)$$

where \bar{v}_j and t_j are the average velocity and the travel time, respectively, between the surface and the bottom of the jth layer. Equation (4) applies only for horizontal layering and only when t_n and t_{n-1} are measured along a ray for which the shot-geophone separation is small enough that sines and tangents of angles of incidence are approximately equal. Since these conditions were satisfied at seismic stations on the Ross Ice Shelf where good I_1W_1 reflections are recorded, equation (4) could be used to calculate the velocity in a sediment layer

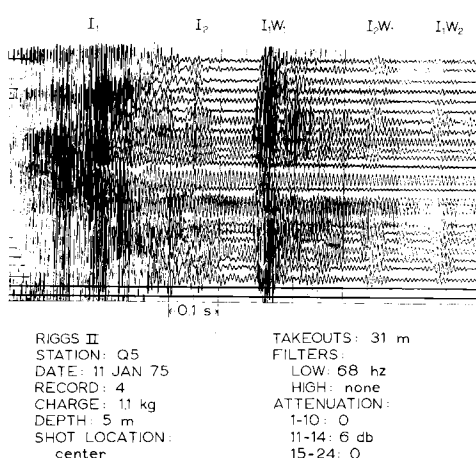


Fig. 22. Seismogram from station Q5 illustrating multiple seismic reflections. I_1 is obscured by direct arrivals through the ice.

TABLE 9. Local Slope of the Seafloor Determined by L Spread Reflection Shooting, Compared With Regional Values

Station	Local Values		Regional Values	
	Strike, deg	Dip	Strike, deg	Dip
H12	225	0.7°N	300	N
IJ9%	325	1.0°S	300	S
JK9%	310	0.3°N	315	none
N4	340	0.7°W	005	W
N5	300	0.4°SW	330	SW
O4	300	0.1°SW	300	N
P5	275	0.8°N	325	N
Q5	200	0.2°E	335	E
RI	270	0.7°S	285	S

Strikes and dips are given as grid azimuths.

below the seafloor if a good reflection from the base of the layer was received.

Good subbottom reflections were recorded at four stations: F9, I11, K11, and M9. (An example is shown in Figure 23.) Travel times, average velocities (determined by the t^2-x^2 method), and interval velocities (v_{sed} , calculated from equation (4)) at the four sites are presented in Table 10. The errors in v_{sed} were calculated from the errors in picking travel times and determining average velocities and do not include the possibility of violation of the assumptions in equation (4).

At stations I11 and M9, v_{sed} (2.5 and 2.6 km s^{-1} , respectively) is consistent with the sediment velocity (2.4 km s^{-1}) computed by Crary [1961] from seismic refraction shooting on sea ice near Little America V Station. Using reflection data, Crary [1961] determined in addition that v_{sed} increased from about 2.1 km s^{-1} at the seafloor to 2.9 km s^{-1} at a depth of 900 m below the seafloor. Similar results have been found from extensive sonobuoy measurements in the Ross Sea [Houtz and Davey 1973; Davey et al., 1983;

Cooper et al., 1987]. Since the velocities at stations I11 and M9 are averages over only the upper 50 m of sediment, it appears that either v_{sed} is slightly higher at these sites than at the sites in the sea north of the ice shelf or there is a slight dip to the layers. The 3.2 km s^{-1} velocity at station K11 is substantially higher than that determined at I11 and M9; in fact, it seems unrealistically high for seafloor sediment, so it probably indicates a dipping subbottom reflector. The velocity calculated at station F9 (1.2 km s^{-1}), on the other hand, is too low to be real, so it is probably also distorted by dip.

Many sampling studies have shown that the sediments on the floor of the Ross Sea consist of poorly sorted clastic deposits of glacial origin [Phillippi, 1912; Stetson and Upson, 1937; Hough, 1950; Thomas, 1959, 1960; Hayes and Frakes, 1975; Barrett and McKelvey, 1981]. Based on the earlier of these analyses and, in particular, on a sediment core near Little America V [Thomas, 1960], Crary correlates his 2.4 km s^{-1} layer with a mixture of coarse and fine glacial till. It is likely that the 2.5 and 2.6 km s^{-1} layers at stations I11 and M9 also are glacial till.

The sediment layer sensed by the subbottom reflections undoubtedly is only a small part

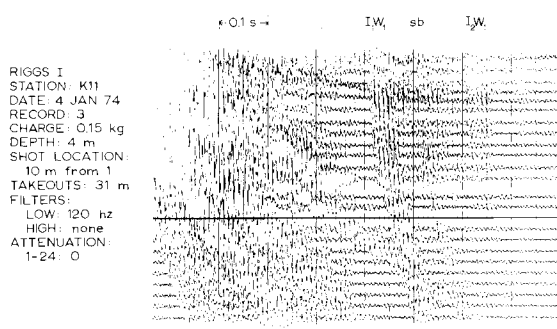


Fig. 23. Seismogram from station K11 illustrating a subbottom reflection ("sb").

TABLE 10. Interval Velocities and Layer Thicknesses, Uppermost Sea Bottom Sediment Layer

Station	Velocity, km s^{-1}	Thickness, m
G9	1.2 ± 0.2	110
I11	2.5 ± 0.2	45
K11	3.2 ± 0.1	156
M9	2.6 ± 0.4	54

of the total sedimentary column at the four RIGGS stations. Long-refraction profiling (see below) in the RIGGS area produces estimates in the range of 500-2000 m for the total thickness of the sedimentary section. Seismic profiler sections of the Ross Sea shelf likewise show that the sedimentary column generally is at least a kilometer thick (summarized by Davey, [1987]). The reflector at 50- to 150-m depth within the sedimentary section beneath the Ross Ice Shelf (Table 10) may correlate with a change in lithology or with an erosional interface. In the Ross Sea a widespread reflector within a few tens of meters of the seafloor (the "Ross Sea unconformity") has been found on profiler records [Houtz and Meijer, 1970; Houtz and Davey, 1973; Karl et al., 1987]. The unconformity was sampled at depths of 20, 20, and 30 m in three of the four holes drilled during Leg 28 of the Deep Sea Drilling Project and determined to be a glacial erosion surface [Hayes and Davey, 1975]. The seismic reflector at the RIGGS stations may be a continuation of the Ross Sea unconformity beneath the ice shelf. Depths to the interface are of the right order, and the ice shelf certainly would have been grounded in the RIGGS area if it were grounded farther to the north.

Sea Bottom Reflection Coefficients and Acoustic Impedances

Robin [1958] has shown that at vertical incidence, the energies per unit area of the I_1 and I_1W_1 reflections at the ice shelf surface are equal to

$$E(I_1) = \frac{E_o r_w^2}{4 h_i} e^{-2\alpha h_i} \quad (5)$$

and

$$E(I_1W_1) = \frac{E_o (1 - r_w^2)^2 r_b^2}{4 [h_i + h_w (v_w/v_p)]^2} e^{-2\alpha h_i} \quad (6)$$

where $E(I_1)$ is the energy of the I_1 reflection, $E(I_1W_1)$ is the energy of the I_1W_1 reflection, E_o is the outgoing energy per unit solid angle, r_w is the (amplitude) reflection coefficient at the ice-water boundary, r_b is the reflection coefficient at the water-sediment boundary, v_w is the sound velocity in seawater, and α is the energy attenuation coefficient in ice (the attenuation in the water is assumed to be negligible). A convenient way to determine r_b from the observed amplitudes of I_1 and I_1W_1

reflections is to take the ratio of equation (5) to equation (6); E_o and α are thus eliminated. The coefficient r_w may be calculated directly from the known velocities and densities of ice and seawater. Once r_b is determined, the acoustic impedance, z_b , of the sediment layer is easily calculated, since

$$z_b = \rho_w v_w \left(\frac{1 + r_b}{1 - r_b} \right) \quad (7)$$

where ρ_w is the density of seawater and $z_b = \rho_{sed} v_{sed}$, ρ_{sed} being the density of the uppermost sediments. Average values of r_b and z_b for nine stations at which both I_1 and I_1W_1 reflections at near-vertical incidence were recorded are listed in Table 11. The data that were used to determine the averages are listed in Table C4 of Appendix C (microfiche).

The differences between the acoustic impedances at the nine sites (Table 11) may result from variations in the lithologies of the upper few meters of bottom sediment. The impedance differences are small, however, and very likely are caused by minor individualities in a single general type of bottom sediment. The average acoustic impedance at the nine sites is $(2.8 \pm 0.2) \text{ Gg m}^{-2} \text{ s}^{-1}$, where ± 0.2 is the standard error of the mean.

The acoustic impedance gives an inverse relationship between v_{sed} and ρ_{sed} , whereas empirical relations between density and velocity in marine sediments, such as those given by Nafe and Drake [1963] and Hamilton [1971, 1982], are direct. Because of that, the two types of relations can be used effectively together to determine ρ_{sed} and v_{sed} separately (Figure 24). The values obtained in this way are $\rho_{sed} = (1.72 \pm 0.11) \text{ Mg m}^{-3}$ and $v_{sed} = (1630 \pm 60) \text{ m s}^{-1}$. This velocity is lower than velocities from the refraction measurements in the Ross Sea cited above, but it refers only to the uppermost few meters of the sedimentary column.

Long-Refraction Studies

Unreversed seismic refraction profiles designed to record acoustic wave arrivals from the bedrock beneath the ice shelf were shot at stations BC, I10S, J9DS, and RI. In this section we present the travel time curves and a discussion of the data analysis. The geological interpretation of the results has already been discussed by Robertson et al. [1982] and is not repeated here. (The seismic interpretations shown here are slightly different from those of Robertson et al. [1982], but they are not different enough

TABLE 11. Sea Bottom Reflection Coefficients (r_b) and Acoustic Impedances (z_b)

Station	n	r_b	z_b' $Gg m^{-2} s^{-1}$
F9	4	0.260 ± 0.013	2.53 ± 0.07
E8	5	0.219 ± 0.014	2.33 ± 0.07
H9S	2	0.442 ± 0.003	3.84 ± 0.03
H11S	2	0.321 ± 0.018	2.89 ± 0.11
L5	2	0.236 ± 0.016	2.41 ± 0.09
N4	6	0.268 ± 0.022	2.59 ± 0.13
N5	3	0.215 ± 0.036	2.32 ± 0.17
P5	2	0.369 ± 0.019	3.23 ± 0.14
Q5	2	0.326 ± 0.004	2.92 ± 0.02
Overall mean		0.295 ± 0.031	2.78 ± 0.20

The numbers listed are the station means, taken from the data in Table D4. Here n is the number of individual measurements of r_b and z_b at each station. The overall means are unweighted, since the values of n are too small to give variances at the individual stations that are meaningful for weighting.

to invalidate their geological interpretation.)

General information about the profiles is presented in Table 12. Distances were either chained (station BC) or measured by Tellurometer (stations I10S, J9DS, and RI). Use of the refraction technique on the ice shelf is complicated by the appreciable thickness of low-velocity seawater and sediments underneath high-velocity ice. Refracted energy

from below the ice is not returned to the surface as a series of first arrivals unless large shot-spread separations are employed, and large distances in turn require large charge sizes.

On all long-refraction profiles there is evidence that a substantial layer of sediments overlies basement on the ocean floor. However, since the wave velocity in the sediment is almost surely less than that in ice, there is no way of measuring it by seismic refraction shooting on the ice shelf. We must assume a velocity; we choose the nearest actual velocity measurement, that by Crary [1961] on the sea ice near Little America V: 2.4 km s^{-1} . (As was pointed out above, our measurements of interval velocity refer only to the uppermost part of the sedimentary column.) To provide an indication of the effect of varying that velocity, we have routinely made calculations for $v_{\text{sed}} = 2.4 \pm 0.4 \text{ km s}^{-1}$ and cited corresponding error bounds on affected thicknesses and depths.

Station BC. The long-refraction shot at BC did not yield a recorded arrival from bedrock (P_g). There are two possible explanations. The first is that the charge size was too small to generate sufficient energy even if the distance was great enough to have recorded P_g as a first arrival. The second is that although the charge was large enough, the distance was too short for P_g to be the first arrival.

One can make a rough calculation to try to determine which of the two explanations is

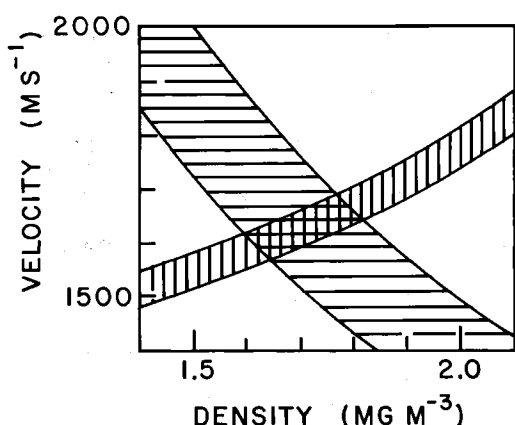


Fig. 24. Velocity versus density in sediments beneath the ice shelf. The zone with horizontal ruling corresponds to $z_b = 2.78 \pm 0.20 \text{ Gg m}^{-2} \text{ s}^{-1}$. The zone with vertical ruling is from Nafe and Drake [1963] and Hamilton [1971, 1982].

TABLE 12. Charge Sizes, Shot Hole Depths, and Distances for Long-Refraction Shooting

Station	Record Number	Shot Hole Depth, m	Charge Size, kg	Distance, km
BC	38	7	91	20.0
I10S	32	9	132	14.5
	33	8	113	12.6
	34	8	91	10.8
J9DS	A15	100	181	21.0
	B9			24.1
RI	A18	15	458	28.0
	B59			26.0
	B60			24.0

more likely. The major factors governing the amount of energy reaching a receiver from a seismic shot are (1) charge size and hole depth, (2) energy loss due to geometrical spreading, (3) energy loss due to attenuation, and (4) energy loss due to reflection at boundaries. The effect of the first factor on the amount of energy generated by a seismic shot in polar firn is poorly known. However, shot 34 at station I10S (Table 12) was the same size charge at nearly the same depth as the BC shot, and a good P_g was recorded from it (Figure 25); so it is convenient to use it as a standard of comparison. Amplitude diminishment from geometrical spreading is approximately inversely proportional to the distance; so the relative value of that factor for BC (compared with I10S) is 0.54. Approximate values of the specific dissipation constant Q^{-1} for ice, seawater, marine sediment, and basement-type rocks are 1.4×10^{-3} [Bentley and Kohnen, 1976], 5×10^{-6} [Bradley and Fort, 1966], 6×10^{-3} [Clay and Medwin, 1977, p. 259], and $(5-20) \times 10^{-4}$ [Bradley and Fort, 1966], respectively; we will use the larger of the figures for basement-type rocks in our calculations. The amplitude attenuation coefficient a for P waves is given by $a = \pi f Q^{-1} / v_p$, where f is the frequency of the signal. From Figure 25 we see that $f \approx 15$ Hz; for bedrock we take $v_p = 5.7 \text{ km s}^{-1}$ (from station I10S). Then $a = 0.017, 1.6 \times 10^{-4}, 0.12$ and 0.017 km^{-1} for ice, water, sediments, and bedrock, respectively. Using these coefficients and known layer thicknesses and distances and assuming the maximum sediment thickness for BC that would allow P_g to be a first arrival at 20 km, we obtain a relative attenuation factor, compared with I10S, of 0.64. Transmission losses have been

calculated from the standard equation (calculable from equation (7)) using $\rho_{\text{sed}} = 2 \text{ Mg m}^{-3}$ and $v_s = 1.2 \text{ km s}^{-1}$ in the sediments; that relative factor amounts to 0.32.

Combining losses, we calculate that the amplitude of a P_g arrival at BC would be about one tenth as large as that at station I10S. Both shots were recorded on the same system at the same gain and filter settings. At station I10S the signal-to-noise ratio (Figure 29, record 34, traces 1-13) is about 10; so at BC the expected signal-to-noise ratio is about 1. Because of the frequency difference between signal and noise, it seems likely that some indication of P_g would have been discernible had it been present. Thus we believe an insufficient shot distance is the more likely explanation for the absence of P_g at BC.

If the shot distance was indeed too small, a minimum thickness of low-velocity sediments, for $v_g = 5.7 \text{ km s}^{-1}$ and $v_{\text{sed}} = 2.4 \pm 0.4 \text{ km s}^{-1}$, is $1.9 \pm 0.4 \text{ km}$.

Station I10S. Station I10S is a grounded station on Crary Ice Rise particularly suited to long-refraction profiling owing to the absence of the water layer. For this profile the geophone spread was fixed and the shots were fired at different locations. For planar interfaces with constant dips across the profile, the apparent velocities across the spread from one shot, and from different shots at the same detector, provide a seismic reversal. In reality, however, the dip under the shots and that under the spread are likely to be different, so neither is well constrained.

The mean apparent velocity for P_g across the records (Figures 25 and 26) from the three shots approximately 2 km apart is $5.72 \pm 0.03 \text{ km s}^{-1}$. The mean is corrected

RIGGS I
 STATION: I10S
 DATE: 13 JAN 74
 RECORD: 32
 CHARGE: 132 kg
 DEPTH: 9 m
 SHOT LOCATION: 14.5 km
 TAKEOUTS: 31 m
 FILTERS:
 LOW: none HIGH: 320 hz
 ATTENUATION:
 1,13: 10 db 2-12,14-24: 0
 HORIZONTAL GEOPHONES:
 LONGITUDINAL: 1,5,9,13,17,21
 TRANSVERSE: 3,7,11,15,19,23

RIGGS I
 STATION: I10S
 DATE: 14 JAN 74
 RECORD: 33
 CHARGE: 113 kg
 DEPTH: 8 m
 SHOT LOCATION: 12.6 km
 TAKEOUTS: 31 m
 FILTERS:
 LOW: none HIGH: 320 hz
 ATTENUATION:
 1-13: 10 db 14-24: 0
 HORIZONTAL GEOPHONES:
 same as record 32

RIGGS I
 STATION: I10S
 DATE: 14 JAN 74
 RECORD: 34
 CHARGE: 91 kg
 DEPTH: 8 m
 SHOT LOCATION: 10.8 km
 TAKEOUTS: 31 m
 FILTERS:
 LOW: none HIGH: 320 hz
 ATTENUATION:
 1-13: 10 db 14-24: 0
 HORIZONTAL GEOPHONES:
 same as record 32

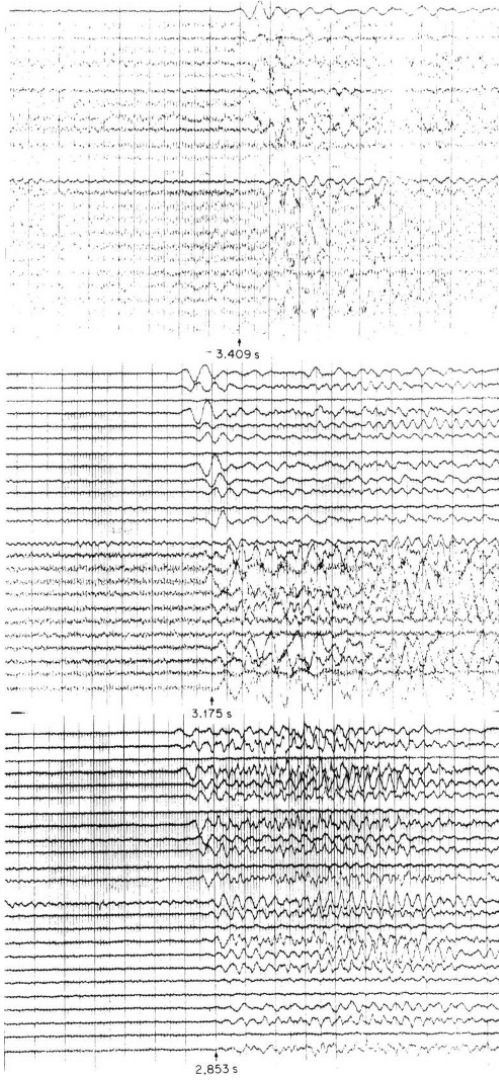


Fig. 25. Long-refraction seismograms from station I10S. Total travel times are marked beneath each seismogram. Shots were grid northwest by north from the recording site.

for a 0.5° slope between top and bottom surfaces of the ice determined by radar sounding. The apparent velocity across all records is close to the mean cross-spread velocity across the three individual records, $5.8 \pm 0.1 \text{ km s}^{-1}$, which implies that there is probably little dip to the basement surface and therefore that 5.7 km s^{-1} is close to the true velocity in the basement.

The travel time intercept determined by least squares regression analysis is $0.92 \pm 0.03 \text{ s}$. The theoretical intercept for ice resting directly on the 5.7 km s^{-1} refractor is only 0.23 s , so a layer of lower velocity must lie in between. The thickness of the

layer can be calculated if a velocity is assumed. For $v_{\text{sed}} = 2.4 \pm 0.4 \text{ km s}^{-1}$, the sediment thickness is $750 \pm 100 \text{ m}$.

Station J9DS. At station J9DS the apparent velocity between two recording points (Figures 27 and 28) 3 km apart is 6.8 km s^{-1} . This velocity is substantially higher than the individual cross-spread velocities calculated for the two spreads: $5.1 \pm 0.2 \text{ km s}^{-1}$ at 21 km and $5.8 \pm 0.2 \text{ km s}^{-1}$ at 24 km. Note that since there was only one shot, the apparent velocities are all affected only by the bedrock dip under and between the two spreads. If we assume that the true velocity in the refractor is 5.7 km s^{-1} , as found at

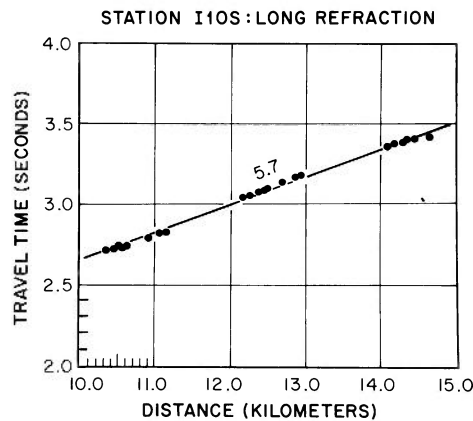


Fig. 26. Long-refraction travel time curve for station I10S. The number on the travel time line is the apparent velocity in kilometers per second.

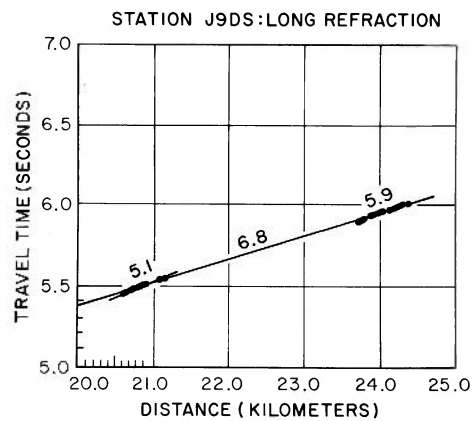


Fig. 28. Long-refraction travel time curve for station J9DS. Numbers above the two sets of points and the line connecting them are apparent velocities in kilometers per second.

RIGGS II
STATION: J9DS
DATE: 2 DEC 74
RECORD: A15
CHARGE: 181 kg
DEPTH: 100 m
SPREAD LOCATION:
21.0 km
TAKEOUTS: 31 m
FILTERS:
LOW: none
HIGH: 320 hz
ATTENUATION: 0
HORIZONTAL
GEOPHONES:
LONGITUDINAL:
16-18, 22-24
TRANSVERSE:
13-15, 19-21

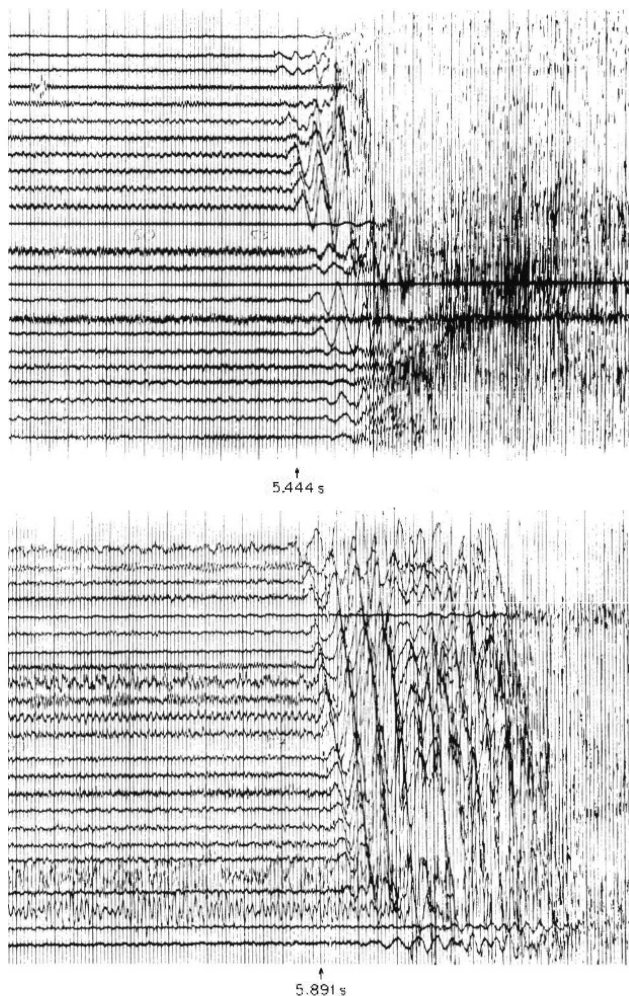


Fig. 27. Long-refraction seismograms from station J9DS. Total travel times are marked beneath each seismogram. The shot was grid east southeast from the recording points.

station I10S 75 km to the grid northeast, then the apparent velocities can be fit by the topography on the refractor shown in Figure 29. (A different wave velocity in the bedrock could be accommodated by a corresponding tilt to the bedrock surface in Figure 29 as a whole.) The full travel time at 24 km (5.98 s) then corresponds to an average sediment thickness of 1.7 ± 0.3 km.

Station RI. Although the first breaks are difficult to pick because the arrival amplitudes are small (Figure 30), there is a recognizable P_g wave group that can be correlated between records. The two peaks of that group are plotted in Figure 31, along with an estimated time for the first breaks. The apparent velocity v_g across the three records is 4.45 ± 0.02 km s $^{-1}$. However, from the minimum intercept time compatible with the known ice and water thicknesses it follows that v_g must actually be at least 4.8 km s $^{-1}$, corresponding to a minimum dip of 2° . But for $v_g = 4.8$ km s $^{-1}$, the overlying sediment layer would have to pinch out at one end of the profile (the sea bottom slope is 0.3°), which is unlikely. It is probable that the sedimentary layer is continuous, so v_g is greater than 4.8 km s $^{-1}$. How much greater it is not possible to determine. For lack of better evidence, we adopt the mean value found by M. P. Hochstein [Robertson et al., 1982] on Roosevelt Island: 5.5 km s $^{-1}$. That yields a mean dip of about 6° under the spreads. The total travel time to 28 km (6.25 s) constrains the sum of the sediment thicknesses beneath the shot and the 28-km spread to be 2.0 ± 0.4 km. If we assume that 1 km of sediment underlies the shot, then the topographic configuration beneath the spreads is as shown in Figure 32.

For ease of comparison, all four seismic sections (including the minimum-depth interpretation at station BC) are shown together in Figure 33.

Summary

Curves of seismic velocity versus depth in the firn, which have been computed from short-refraction travel time data at nine sites, possess the same smoothly varying curved shape, concave toward the depth axis, that has been found previously to be characteristic of the seismic velocity-depth function in ice sheets; v_p increases from about 500 m s $^{-1}$ at the surface to 3800 m s $^{-1}$ at depths of 70 or 80 m, and v_s ranges from about 300 m s $^{-1}$ at the surface to about 1970 m s $^{-1}$ at 60 m.

Recrystallization and densification of firn, which increase v_p and v_s , and increasing temperature with depth, which

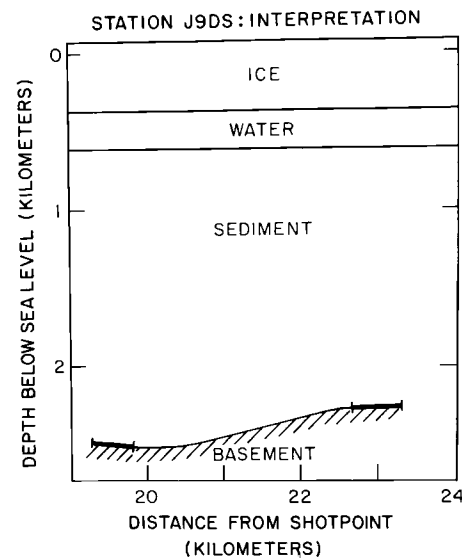


Fig. 29. Seismic interpretation at station J9DS.

decrease both velocities, interact in the ice shelf to produce maximum velocities at a depth of about 100 m. Maximum v_p , as determined by three different methods, is 3811 ± 7 m s $^{-1}$, which is significantly lower than the average in grounded ice sheets (3850 m s $^{-1}$) at the same mean annual surface temperature. The reason for the difference has not yet been ascertained. At stations BC and RI, where the profiles were reversed, it appears that planes of constant velocity dip a few tenths of a degree.

The mean of $15 t^2-x^2$ determinations of \bar{v}_p in the ice shelf is 3688 ± 15 m s $^{-1}$. The scatter of the data is too large to verify the expected dependence of \bar{v}_p on ice thickness.

Densities measured on a 100-m ice core obtained at station J9DS show good agreement with densities computed from the v_p versus depth curve at the same site from the equation of Kohnen [1972]. Kohnen's equation was therefore used to calculate densities at other geophysical stations lacking direct measurements; then ρ , v_p , and v_s were used to calculate Poisson's ratio, Young's modulus, the shear modulus, Lamé's modulus, and the bulk modulus as functions of density. The calculated values of the elastic moduli in solid ice are all consistent with values computed for idealized, nonporous, isotropic, polycrystalline ice from experimental data on acoustic velocities in single ice crystals.

Significant depths in the densification process of the firn may be located by approximating segments of dv_p/dx versus z

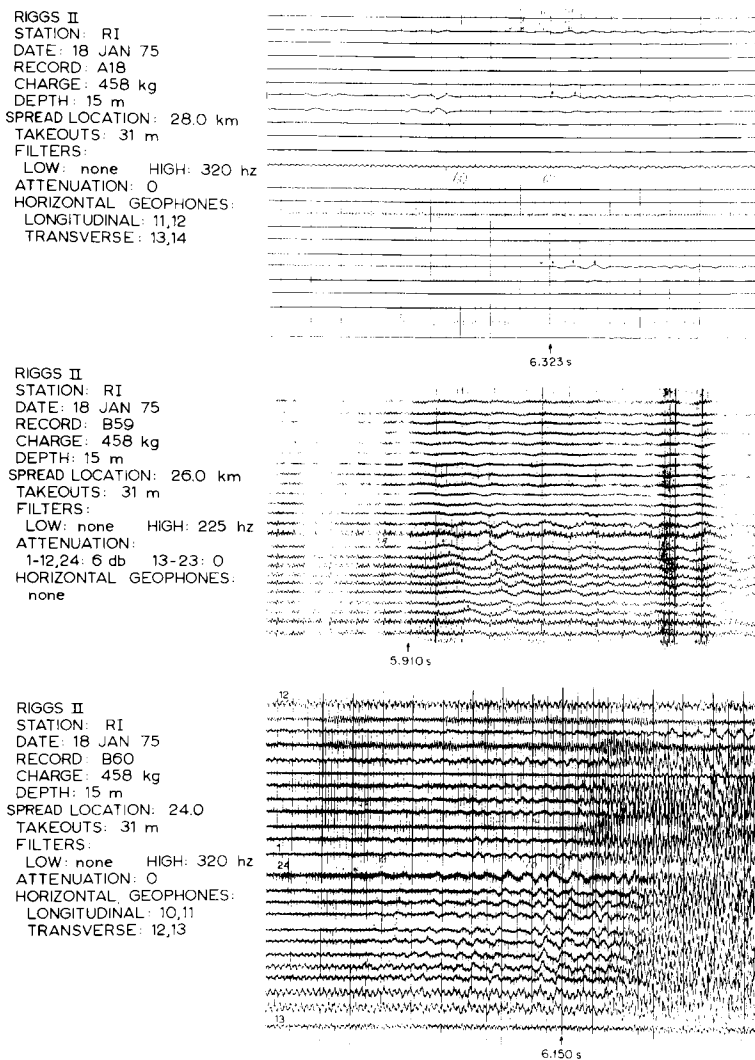


Fig. 30. Long-refraction seismograms from station RI. Note the unexpected numbering of traces corresponding to geophones 1-12 and 13-24 on record B60. Total travel times are marked at the bottom of each seismogram. The shot was grid southeast from the recording points.

with exponential functions. Mean depths to seismic horizons B (the limit of grain boundary sliding), C (glaciological significance unknown), and D (the firn-ice boundary) are 11 ± 2 m, 25 ± 10 m, and 46 ± 8 m, respectively. A curve of dv_z/dz versus z averaged over all stations does not show horizon C, a fact that is consistent with the low measured rates of snow accumulation on the ice shelf.

There is no overall mean difference between ice thicknesses calculated from radar echo times and those calculated from seismic reflections, although there is an unexplained

suggestion that the mean difference for RIGGS I is 10 m or so greater than that for RIGGS II. Discrepancies between short-refraction SH and SV profiles at station RI are consistent with anisotropic snow structure in the top few meters of snow and with a zone of anisotropy, due perhaps to high longitudinal strain rates or an abundance of horizontal ice lenses, between 10 and 25 m.

The slopes of the seafloor at the nine stations where they were determined are all no greater than 1° . It appears that bottom slope is a negligible source of error in the measurement of sea bottom elevation by

reflections shooting and in the determination of gravity anomalies.

Interval velocities in the layer of sediment at the seafloor match those expected for unconsolidated glacial marine till. The subbottom reflecting interface lies within the total sedimentary section at a depth of 50-150 m below the seafloor and may correlate with the glacial erosional surface identified on profiler records as widespread in the Ross Sea and sampled during Leg 28 of the Deep Sea Drilling Project. The mean acoustic impedance of the bottom sediment at nine stations is $2.8 \pm 0.2 \text{ Gg m}^{-2} \text{ s}^{-1}$. Together with a standard curve of velocity versus density in marine sediments, this yields $\rho = 1.7 \pm 0.1 \text{ Mg m}^{-3}$ and $v_{\text{sed}} = 1630 \pm 120 \text{ m s}^{-1}$; these also are consistent with a layer of unconsolidated glacial marine material at the seafloor.

Long-refraction shooting was carried out at four sites, with results summarized in Figure 33. At station BC, wave arrivals from bedrock were not recorded. The velocity in seismic basement on Crary Ice Rise (station I10S) is 5.7 km s^{-1} . A layer of lower velocity lies between the bottom of the ice and the basement; if a velocity in the layer of $2.4 \pm 0.4 \text{ km s}^{-1}$ is assumed, its calculated thickness on Crary Ice Rise is $750 \pm 100 \text{ m}$.

Apparent velocities in basement at station

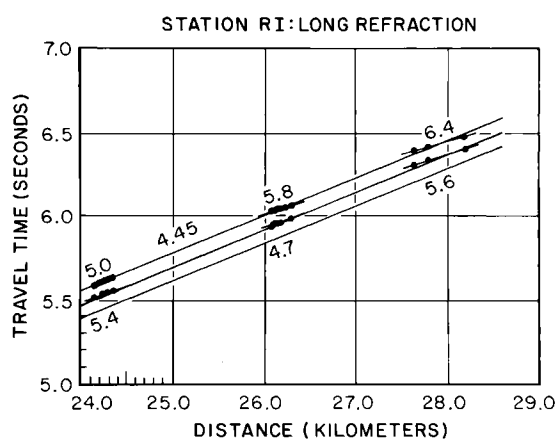


Fig. 31. Long-refraction travel time curve for station RI. The upper and lower sets of points correspond to the first two wave peaks in the refracted arrival. Numbers above and below the six sets of points and above the line connecting the upper three are apparent velocities. The lowest of the three parallel travel time lines approximately connects first arrival times.

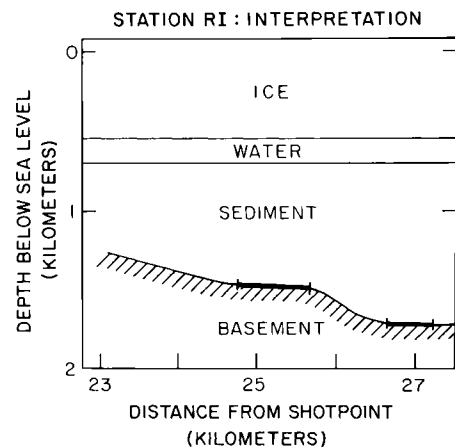


Fig. 32. Seismic interpretation at station RI.

J9DS range from 5.0 to 6.8 km s^{-1} . The scatter probably is caused by topography along the refractor. Since J9DS is close to I10S, the true velocity in basement may be about 5.7 km s^{-1} ; if so, the seismic interpretation is characterized by a layer of sediments $1.7 \pm 0.3 \text{ km}$ thick and a mean 4° slope on the basement surface.

At station RI, if we assume that the true velocity in seismic basement is about 5.5 km s^{-1} , as appears likely from work on nearby Roosevelt Island, the dip along the refractor is about 6° , and an average of $1.0 \pm 0.4 \text{ km}$ of sediment lies between the sea bottom and the refractor.

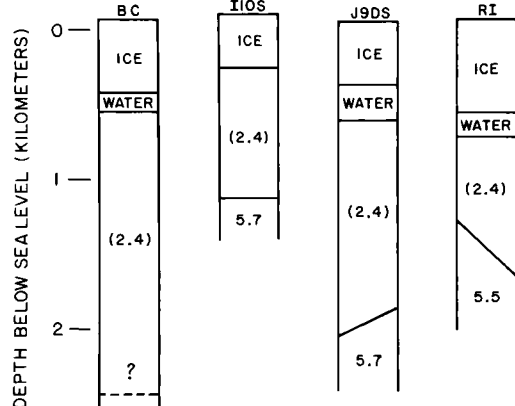


Fig. 33. Comparison of seismic interpretations at stations BC, I10S, J9DS, and RI. Values in parentheses denote assumed velocities.

Acknowledgments. During RIGGS I, the field party comprised C. R. Bentley (leader), S. Brandwein, J. W. Clough, T. Kolich, J. D. Robertson, B. K. Sternberg, and L. R. Whiting. For RIGGS II, Clough was the leader; Kolich, Robertson, and Whiting returned, and the other members were D. Borowski, K. C. Jezek, and J. F. Kirchner. The data on which this paper is based could never have been gathered without the tireless efforts of those field party members. We are especially grateful to J. W. Clough both for his valuable assistance in the field and his many helpful suggestions in the analysis of the data. R. H. Thomas and coworkers from the University of Nebraska assisted us by making electronic distance measurements for our seismic profiles. Logistic support was provided by the Ross Ice Shelf Project Management Office, Holmes and Narver, Inc., United States Naval Support Force, Antarctica, and Antarctic Development Squadron Six. We thank P. Dombrowski and S. H. Werther for drafting illustrations and A. N. Mares and J. V. Campbell for manuscript preparation. This work was supported by the National Science Foundation under grants DPP72-05802, DPP79-20736, and DPP-8119989. This is contribution 490 of the Geophysical and Polar Research Center, University of Wisconsin-Madison.

References

- Albert, D. G., and C. R. Bentley, Seismic studies on the grid eastern half of the Ross Ice Shelf: RIGGS III and RIGGS IV, in The Ross Ice Shelf: Glaciology and Geophysics, Antarct. Res. Ser., vol. 42, edited by C. R. Bentley and D. E. Hayes, AGU, Washington, D. C., this volume.
- Alley, R. B., Firn densification by grain-boundary sliding: A first model, J. Phys. Colloq. C1, Suppl. 3, 48, C1-249-C1-256, 1987a.
- Alley, R. B., Texture of polar firn for remote sensing, Ann. Glaciol., 9, 1-4, 1987b.
- Anderson, D. L., and C. S. Benson, The densification and diagenesis of snow, in Ice and Snow, edited by W. D. Kingery, pp. 391-411, MIT Press, Cambridge, Mass., 1963.
- Barrett, P. J., and B. C. McKelvey, Cenozoic and tectonic history of the Transantarctic Mountains in the McMurdo Sound area, recent progress from drilling and related studies, Polar Rec., 20, 543-548, 1981.
- Bennett, H. F., An investigation into velocity anisotropy through measurements of ultrasonic wave velocities in snow and ice cores from Greenland and Antarctica, Ph.D. dissertation, Univ. of Wis., Madison, Wis., 1968.
- Bennett, H. F., Measurements of ultrasonic wave velocities in ice cores from Greenland and Antarctica, Res. Rep. 237, U.S. Army Cold Regions Research and Eng. Lab., Hanover, N. H., 1972.
- Bentley, C. R., Structure of Antarctica and its ice cover, in Research in Geophysics, vol. 2: Solid Earth and Interface Phenomena, edited by H. Odishaw, pp. 335-389, MIT Press, Cambridge, Mass., 1964.
- Bentley, C. R., Seismic anisotropy in the West Antarctic ice sheet, in Antarctic Snow and Ice Studies II, Antarct. Res. Ser., vol. 16, edited by A. P. Cray, pp. 131-177, AGU, Washington, D. C., 1971.
- Bentley, C. R., Seismic wave velocities in anisotropic ice: A comparison of measured and calculated values in and around the deep drill hole at Byrd Station, Antarctica, J. Geophys. Res., 77, 4406-4420, 1972.
- Bentley, C. R., The Ross Ice Shelf Geophysical and Glaciological Survey (RIGGS): Introduction and summary of measurements performed, in The Ross Ice Shelf: Glaciology and Geophysics, Antarct. Res. Ser., vol. 42, edited by C.R. Bentley and D.E. Hayes, pp. 1-20, AGU, Washington, D. C., 1984.
- Bentley, C. R., and K. C. Jezek, RISS, RISP, and RIGGS: Post-IGY glaciological investigations of the Ross Ice Shelf in the U.S. program, J. R. Soc. N. Z., 11, 355-372, 1981.
- Bentley, C. R., and H. Kohnen, Seismic refraction measurements of internal friction in Antarctic ice, J. Geophys. Res., 81, 1519-1526, 1976.
- Bentley, C. R., P. W. Pomeroy, and H. J. Dorman, Seismic measurements on the Greenland ice cap, Ann. Geophys., 13, 253-285, 1957.
- Bentley, C. R., J. W. Clough, K. C. Jezek, and S. Shabtaie, Ice thickness patterns and the dynamics of the Ross Ice Shelf, J. Glaciol., 24, 287-294, 1979.
- Bentley, C. R., S. Shabtaie, D. D. Blankenship, S. T. Rooney, D. G. Schultz, S. Anandakrishnan, and R. B. Alley, Remote sensing of the Ross ice streams and adjacent Ross Ice Shelf, Antarctica, Ann. Glaciol., 9, 20-29, 1987.
- Bradley, J. J., and A. N. Fort, Jr., Internal friction in rocks, in Handbook of Physical Constants, Mem. 97, edited by S. P. Clark, pp. 175-195, Geological Society of America, Boulder, Colo., 1966.
- Brockamp, B., and P. Pistor, Ein Beitrag zur seismischen erforschung der struktur des Gronlandschen inländiseis, Polarforschung, 6, 133-146, 1967.

- Brockamp, B., and H. Querfurth, Untersuchungen über die elastizitätskonstanten von see und kunsteis, Polarforschung, 5, 253-262, 1964.
- Clausen, H. B., W. Dansgaard, J. Nielson, and J. W. Clough, The surface accumulation on the Ross Ice Shelf, Antarct. J. U. S., 14, 68-72, 1979.
- Clay, C. S., and H. Medwin, Acoustical Oceanography, 544 pp., John Wiley, New York, 1977.
- Clough, J. W., and C. R. Bentley, Measurements of electromagnetic wave velocity in the East Antarctic ice sheet, IASH Publ., 86, 115-128, 1970.
- Clough, J. W., and B. L. Hansen, The Ross Ice Shelf Project, Science, 203, 433-434, 1979.
- Cooper, A. K., F. J. Davey, and J. C. Behrendt, Seismic stratigraphy and structure of the Victoria Land basin, western Ross Sea, Antarctica, in The Antarctic Continental Margin: Geology and Geophysics of the Western Ross Sea, CPCEMR Earth Sci. Ser., vol. 5B, pp. 27-76, Circum-Pacific Council for Energy and Mineral Resources, Houston, Texas, 1987.
- Crary, A. P., Marine sediment thickness in the eastern Ross Sea area, Antarctica, Geol. Soc. Am. Bull., 72, 787-790, 1961.
- Crary, A. P., E. S. Robinson, H. F. Bennett, and W. W. Boyd, Jr., Glaciological studies of the Ross Ice Shelf, Antarctica, 1957-1960, IGY Glaciol. Rep. 6, Am. Geogr. Soc., New York, 1962a.
- Crary, A. P., E. S. Robinson, H. F. Bennett, and W. W. Boyd, Jr., Glaciological regime of the Ross Ice Shelf, J. Geophys. Res., 67, 2791-2807, 1962b.
- Davey, F. J., Geology and structure of the Ross Sea Region, in The Antarctic Continental Margin: Geology and Geophysics of the Western Ross Sea, CPCEMR Earth Sci. Ser., vol. 5B, 1-15, Circum-Pacific Council for Energy and Mineral Resources, Houston, Texas, 1987.
- Davey, F. J., K. Hinz, and H. Schroeder, Sedimentary basins of the Ross Sea, Antarctica, Antarctic Earth Science, edited by R. L. Oliver, P. R. James, and J. B. Jago, pp. 533-538, Australian Academy of Science, Canberra, 1983.
- Dix, C. H., Seismic velocities from surface measurements, Geophysics, 20, 68-86, 1955.
- Dobrin, M. B., Introduction to Geophysical Prospecting, 446 pp., McGraw-Hill, New York, 1960.
- Gow, A. J., The inner structure of the Ross Ice Shelf at Little America V, Antarctica, as revealed by deep core drilling, IASH Publ., 61, 272-284, 1963.
- Gow, A. J., Deep core studies of the accumulation and densification of snow at Byrd Station and Little America V, Antarctica, Res. Rep. 197, U.S. Army Cold Regions Res. and Eng. Lab., Hanover, N. H., 1968.
- Gow, A. J., Deep core studies of the crystal structure and fabrics of Antarctic glacier ice, Res. Rep. 282, U.S. Army Cold Regions Res. and Eng. Lab., Hanover, N. H., 1970a.
- Gow, A. J., Preliminary results of studies of ice cores from the 2164 m deep drill hole, Byrd Station, Antarctica, IASH Publ., 86, 78-90, 1970b.
- Gow, A. J., and T. Williamson, Rheological implications of the internal structure and crystal fabrics of the West Antarctic ice sheet as revealed by deep core drilling at Byrd Station, Res. Rep. 76-35, U.S. Army Cold Regions Res. and Eng. Lab., Hanover, N. H., 1976.
- Grant, F. S., and G. F. West, Interpretation Theory in Applied Geophysics, 583 pp., McGraw-Hill, New York, 1965.
- Greischar, L. L., and C. R. Bentley, Isostatic equilibrium grounding line between the West Antarctic ice sheet and the Ross Ice Shelf, Nature, 283, 651-654, 1980.
- Hamilton, E. L., Prediction of in-situ acoustic and elastic properties of marine sediments, Geophysics, 36, 266-284, 1971.
- Hamilton, E. L., Sound velocity and related properties of marine sediments, J. Acoust. Soc. Am., 72, 1891-1904, 1982.
- Hayes, D. E., and F. J. Davey, A geophysical study of the Ross Sea Antarctica, Initial Rep. Deep Sea Drill. Proj., 28, 887-907, 1975.
- Hayes, D. E. and L. A. Frakes, General synthesis, Initial Rep. Deep Sea Drill. Proj., 28, 919-942, 1975.
- Hough, J. L., Pleistocene lithology of Antarctic ocean bottom sediments, J. Geol., 58, 254-260, 1950.
- Houtz, R., and F. J. Davey, Seismic profiler and sonobuoy measurements in Ross Sea, Antarctica, J. Geophys. Res., 78, 3448-3468, 1973.
- Houtz, R., and R. Meijer, Structure of the Ross Sea shelf from profiler data, J. Geophys. Res., 75, 6592-6597, 1970.
- Jiracek, G. R., Radio sounding of Antarctic ice, Res. Rep. 67-1, Univ. of Wis., Madison, Wis., 1967.
- Jiracek, G. R., and C. R. Bentley, Velocity of electromagnetic waves in Antarctic ice, in Antarctic Snow and Ice Studies II, Antarct. Res. Ser., vol. 16, edited by A. P. Crary, pp. 199-208, AGU, Washington, D. C., 1971.
- Johari, G. P., and S. J. Jones, The orientation polarization in hexagonal ice parallel and perpendicular to the c-axis, J. Glaciol., 21, 259-276, 1978.

- Karl, H. A., E. Reimnitz, and B. D. Edwards, Extent and nature of the Ross Sea unconformity in the western Ross Sea, Antarctica, in The Antarctic Continental Margin: Geology and Geophysics of the Western Ross Sea, CPCEMR Earth Sci. Ser., vol. 5B, pp. 77-92, Circum-Pacific Council for Energy and Mineral Resources, Houston, Texas, 1987.
- Kirchner, J. F., and C. R. Bentley, RIGGS III: Seismic short-refraction studies using an analytical curve-fitting technique, in The Ross Ice Shelf: Glaciology and Geophysics, Antarct. Res. Ser., vol. 42, edited by C. R. Bentley and D. E. Hayes, AGU, Washington, D. C., this volume.
- Kohnen, H., Über die beziehung zwischen seismischen geschwindigkeiten und der dichte in firn und eis, Z. Geophys., 38, 925-935, 1972.
- Kohnen, H., The temperature dependence of seismic waves in ice, J. Glaciol., 13, 144-147, 1974.
- Kohnen, H., and C. R. Bentley, Seismic refraction and reflection measurements at Byrd Station, Antarctica, J. Glaciol., 12, 101-111, 1973.
- Kohnen, H., and C. R. Bentley, Ultrasonic measurements on ice cores from the RISP drill hole, Ross Ice Shelf, Antarctica, Antarct. J. U. S., 12, 148-150, 1977.
- Kohnen, H., and A. J. Gow, Ultrasonic velocity investigations of crystal anisotropy in deep ice cores from Antarctica, J. Geophys. Res., 84, 4865-4874, 1979.
- Langway, C. C., Jr., Antarctic ice core studies, Antarct. J. U. S., 10, 152-153, 1975.
- Mellor, M., Snow and ice on the Earth's surface, Monogr. II-C, 163 pp., U.S. Army Cold Regions Res. and Eng. Lab., Hanover, N. H., 1964.
- Nafe, J. E., and C. L. Drake, Physical properties of marine sediments, in The Sea, vol. 1, edited by M. N. Hill, pp. 794-815, John Wiley, New York, 1963.
- Neal, C. S., Dynamics of the Ross Ice Shelf as revealed by radio echo sounding, J. Glaciol., 24, 295-307, 1979.
- Phillippi, E., Die grundproben der Deutschen Sudpolar-Expedition 1901-03, Dtsch. Subpolar Exped., 2, 411-616, 1912.
- Robertson, J. D., Geophysical studies on the Ross Ice Shelf, Antarctica, Ph.D. thesis, 214 pp., Univ. of Wis., Madison, Wis., 1975.
- Robertson, J. D., and C. R. Bentley, Investigation of polar snow using seismic velo-
- city gradients, J. Glaciol., 14, 39-48, 1975.
- Robertson, J. D., C. R. Bentley, J. W. Clough, and L. L. Greischar, Sea-bottom topography and crustal structure below the Ross Ice Shelf, Antarctica, in Antarctic Geoscience, edited by C. Craddock, pp. 1083-1090, University of Wisconsin Press, Madison, Wis., 1982.
- Robin, G. de Q., Seismic shooting and related investigations, in Norwegian-British-Swedish Antarctic Expedition, 1949-51, Scientific Results V, Glaciology III, 134 pp., Norsk Polarinstitutt, Oslo, 1958.
- Robin, G. de Q., Velocity of radio waves in ice by means of a borehole interferometric technique, J. Glaciol., 15, 151-160, 1975.
- Robin, G. de Q., S. Evans, and J. T. Bailey, Interpretation of radio echo sounding in polar ice sheets, Philos. Trans. R. Soc. London, Ser. A, 265, 437-505, 1969.
- Roethlisberger, H., Seismic exploration in cold regions, Monogr. II-A2a, U.S. Army Cold Regions Res. and Eng. Lab., Hanover, N. H., 1972.
- Shabtaie, S., and C. R. Bentley, Tabular icebergs: Implication from geophysical studies of ice shelves, J. Glaciol., 28, 413-430, 1982.
- Stetson, H. C., and J. E. Upson, Bottom deposits of the Ross Sea, J. Sediment. Petrol., 7, 55-66, 1937.
- Thiel, E., and J. C. Behrendt, Seismic studies on the Filchner Ice Shelf, Antarctica, 1957-58, IGY Glaciol. Rep. 2, Am. Geogr. Soc., New York, 1959.
- Thiel, E., and N. A. Osteno, Seismic studies on Antarctic ice shelves, Geophysics, 26, 706-715, 1961.
- Thomas, C. W., Lithology and zoology of an Antarctic Ocean bottom core, Deep Sea Res., 6, 5-15, 1959.
- Thomas, C. W., Late Pleistocene and Recent limits of the Ross Ice Shelf, J. Geophys. Res., 65, 1789-1792, 1960.
- Thomas, R. H., The distribution of 10-m temperatures on the Ross Ice Shelf, J. Glaciol., 16, 111-117, 1976.
- Thomas, R. H., D. R. MacAyeal, D. H. Eilers, and D. R. Gaylord, Glaciological studies on the Ross Ice Shelf, Antarctica, 1973-1978, in The Ross Ice Shelf: Glaciology and Geophysics, Antarct. Res. Ser., vol. 42, edited by C. R. Bentley and D. E. Hayes, pp. 21-53, AGU, Washington, D. C., 1984.

(Received December 23, 1987;
revised August 18, 1989;
accepted November 22, 1989.)